Nanomanufacturing
University of Michigan
ME599-002 | Winter 2010

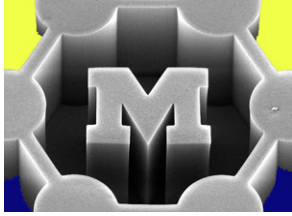

11: Surface plasmon resonance and energy transfer

February 17, 2010

John Hart, Aaron Schmidt
ajohnh@umich.edu
http://www.umich.edu/~ajohnh

Announcements

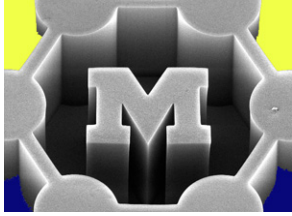

- PS2 due Monday 10.40am
  - No lecture Monday
    - Put your HW in box outside John's office (2278 GGB)
    - Use the time to work on the video assignment!
  - Later lecture schedule to be revised
- Sign up for video topic no later than Monday
- Project description coming next week
- March will be a busy month (project proposal, PS3, video, exam)

Recap: electrostatics in solution

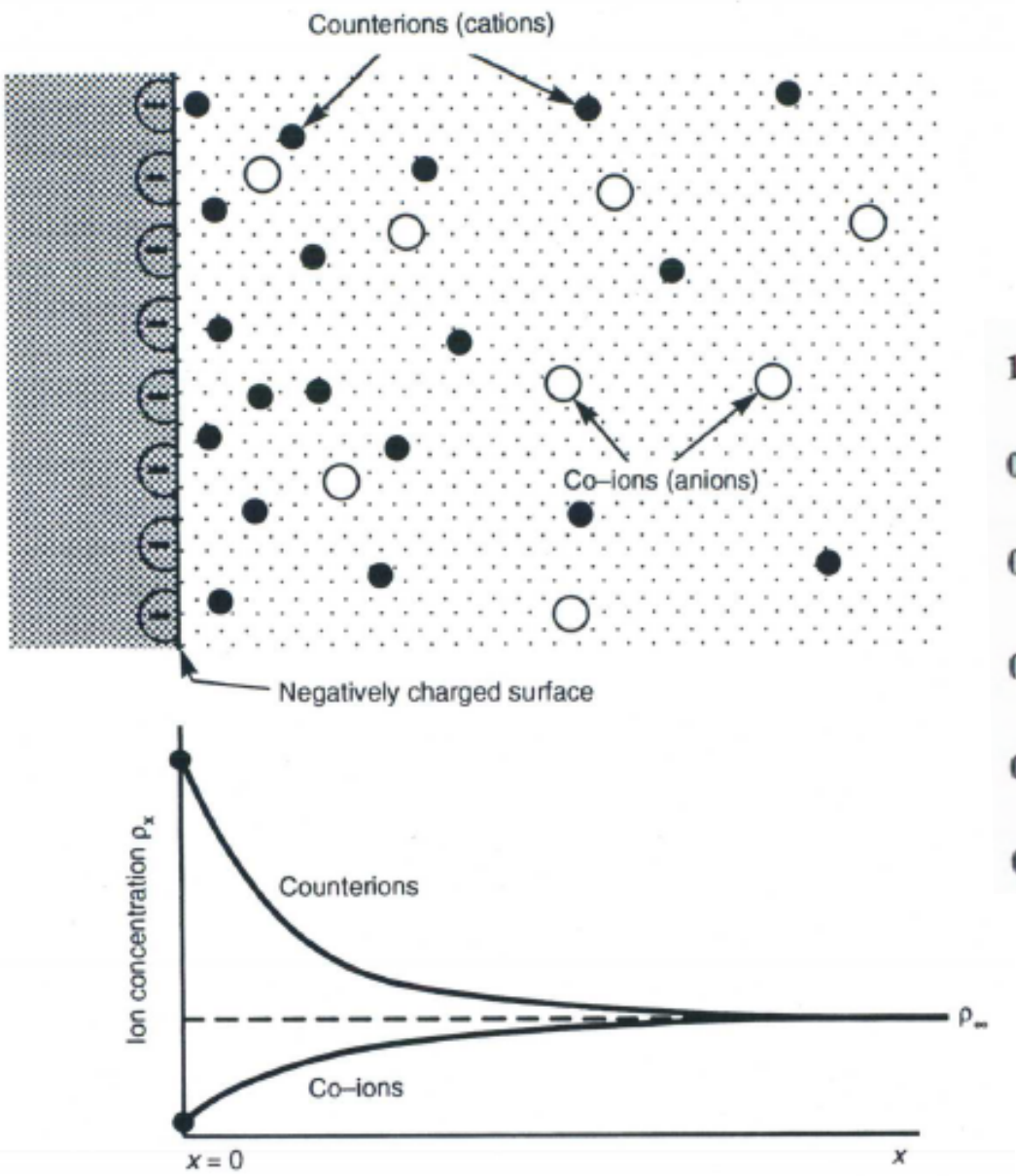

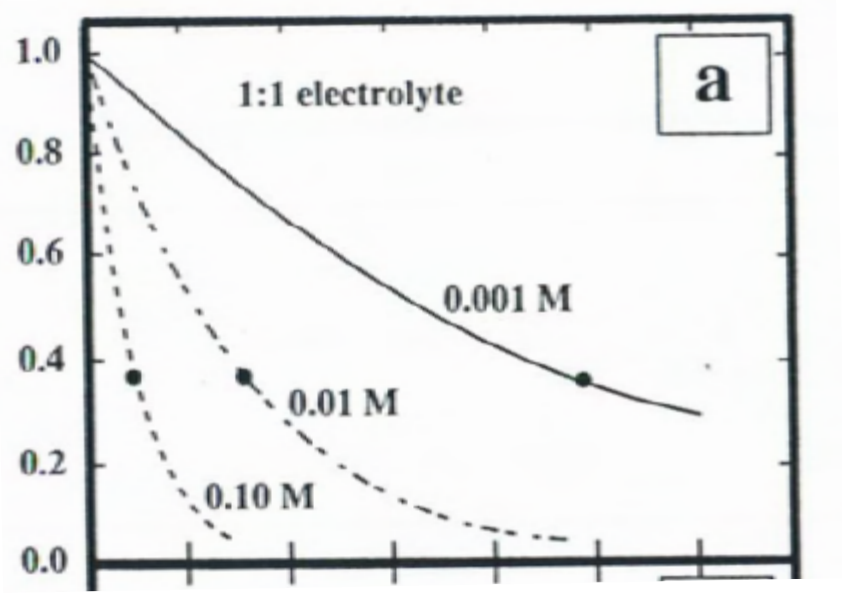

Israelachvili, Mulvaney.

Stabilization of colloids: DLVO theory

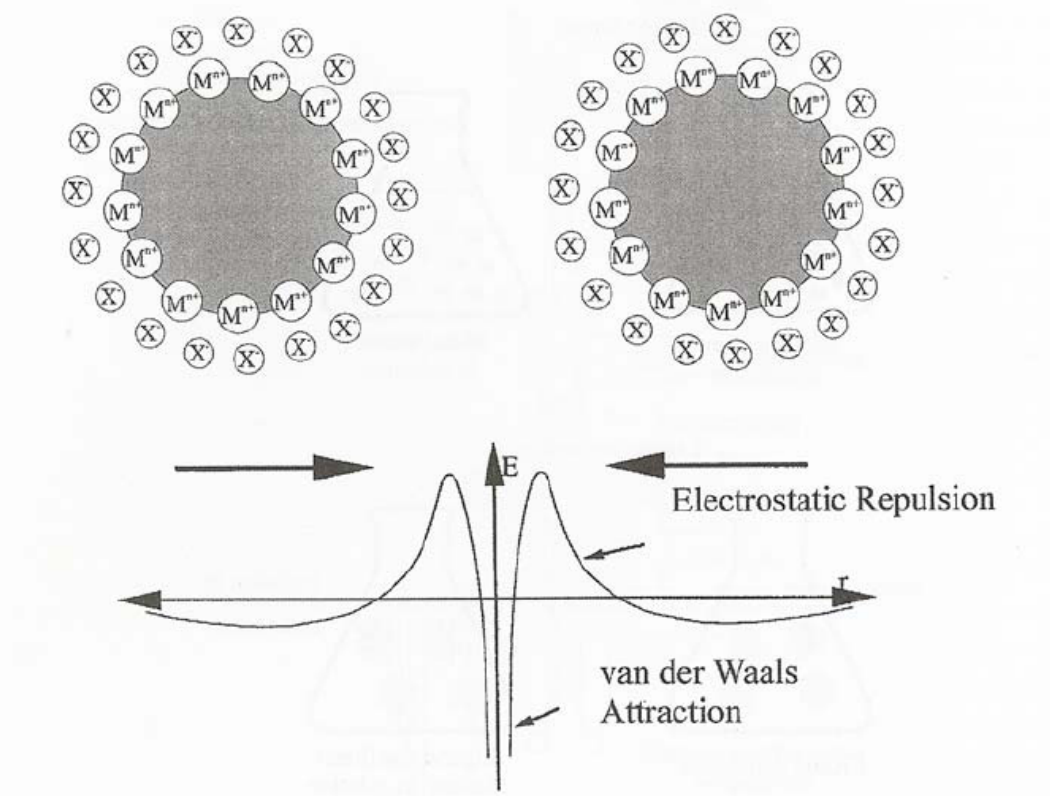

FIGURE 2.24 Electrostatic stabilization of metal colloids. Van der Waals attraction and electrostatic repulsion compete with each other.[27]

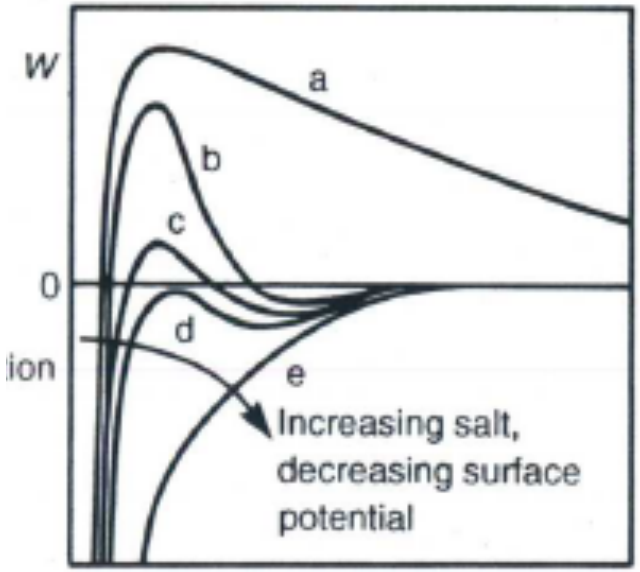

Example: interaction between a pair of Au particles

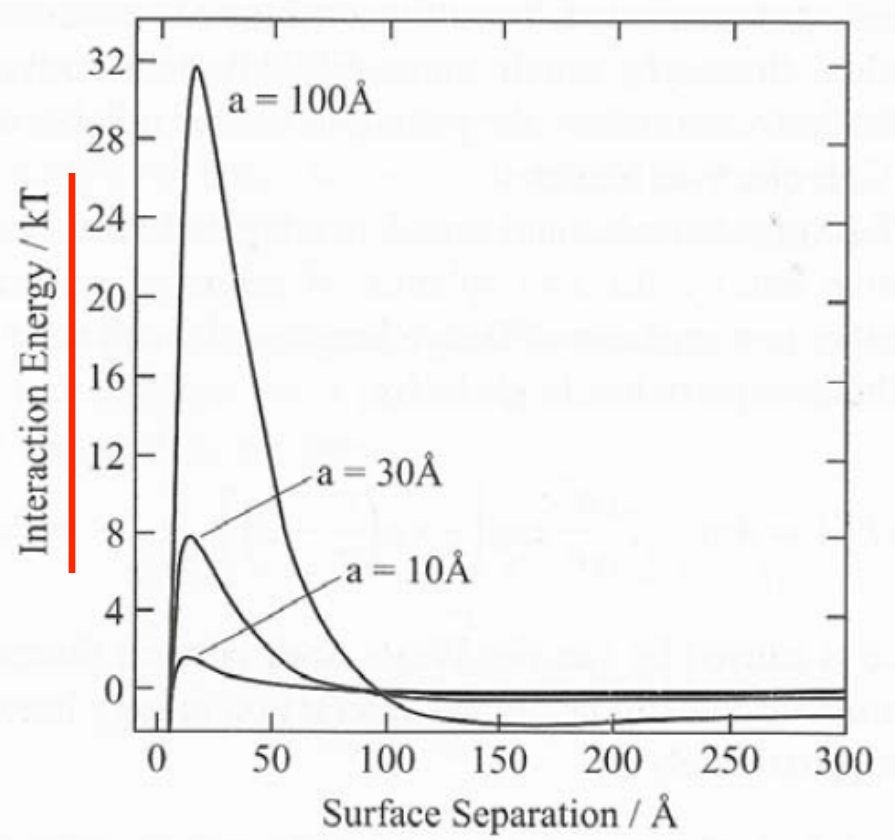

FIGURE 5.4 Plot of the interaction energy between two spherical gold particles in aqueous solution as a function of the particle separation, for several particle radii. Hamaker constant $= 25 \times 10^{-20}$ J, $I = 1$ mM, $\psi_0 = 0.10$ V, $a = 1.0$ nm, 3.0 nm, and 10.0 nm, Debye length = 10 nm. Note that the secondary minimum is negligible for nanoparticles, but becomes important above 10 nm.

Mulvaney.

Diffuse layer and Stern layer

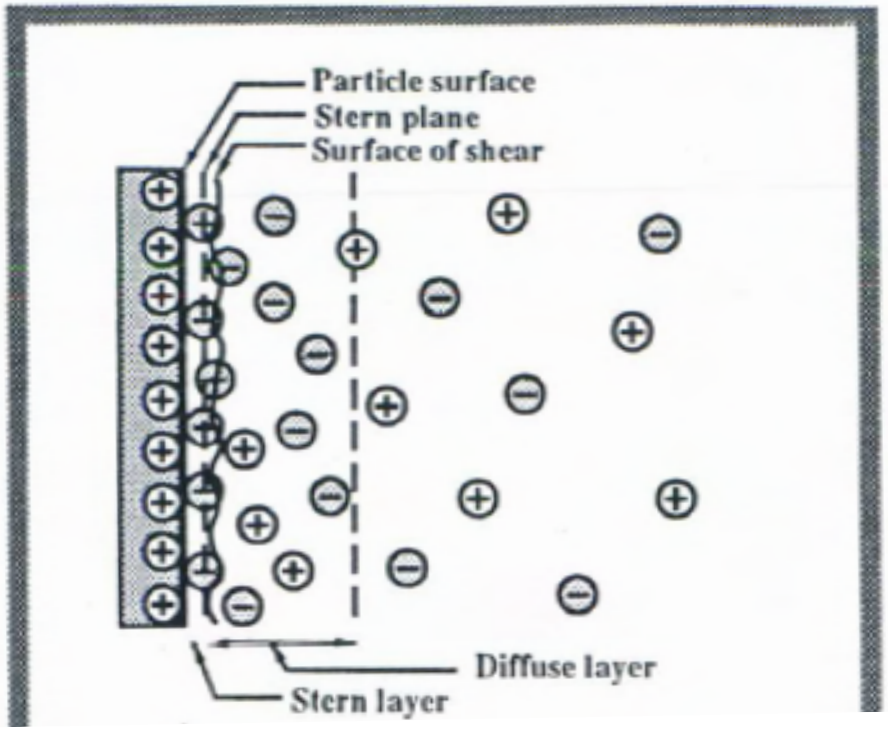

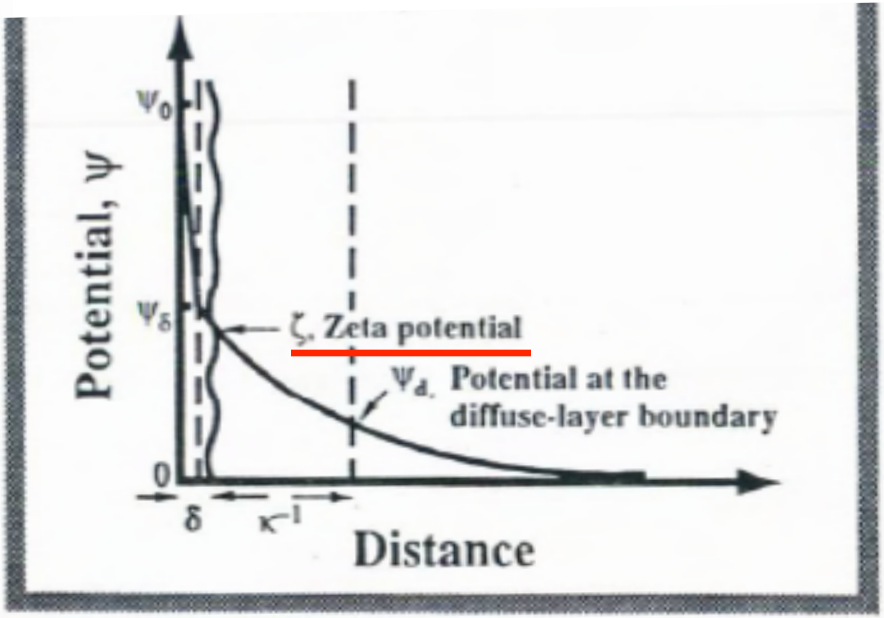

FIG. 11.9 Schematic illustration of the variation of potential the presence of a Stern layer. See Chapter 12 for discussion of s

- Zeta potential is typically measured
- Think about slip..

Hiemenz and Rajagopalan.

Overlapping double layers in a nanogap

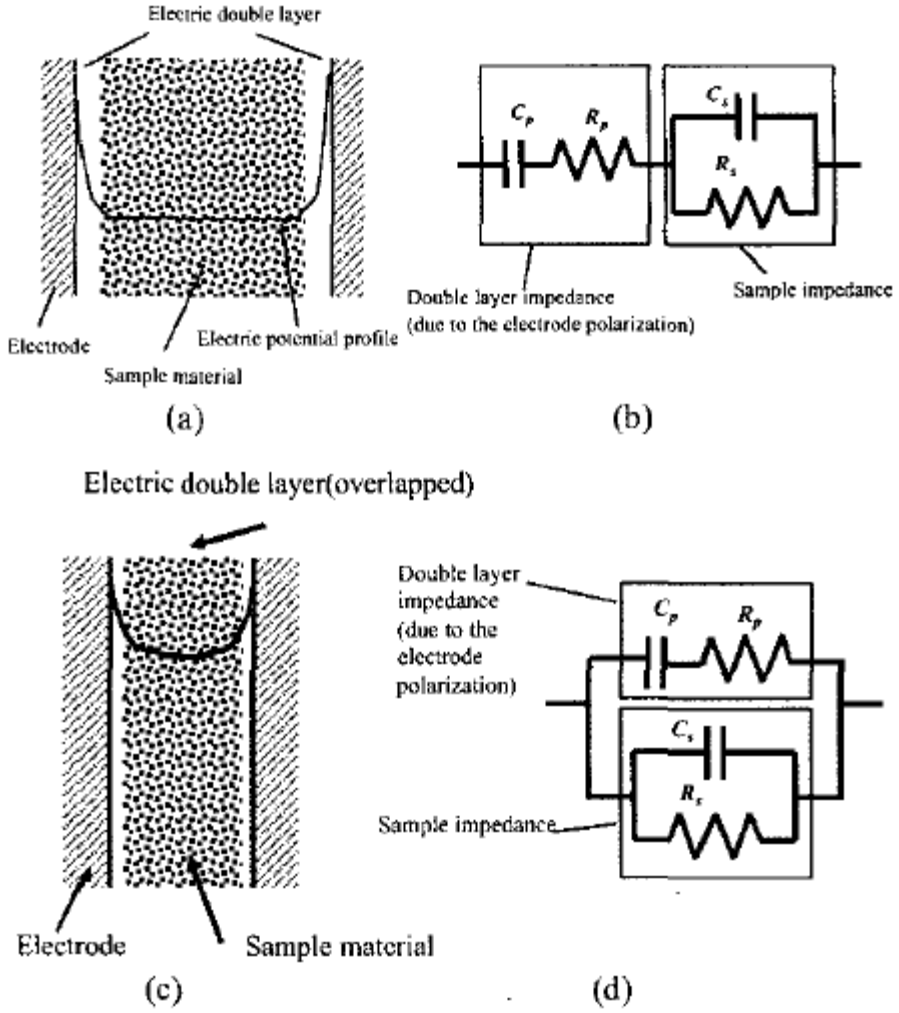

Figure 1: Schematic diagram and equivalent circuits of conventional electrode polarization (a) & (b) and nanogap electrodes (c) & (d).

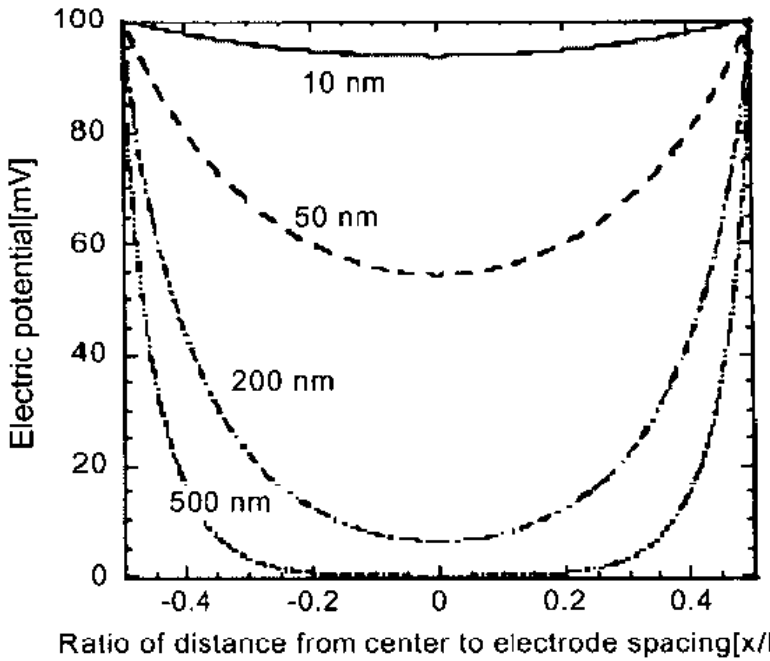

Figure 5: Electric potential between two electrodes for various channel width; the concentration of solution is 0.1mM of 1:1 electrolyte.

Oh et al., IEEE MEMS 03.

Nanofluidic transistors

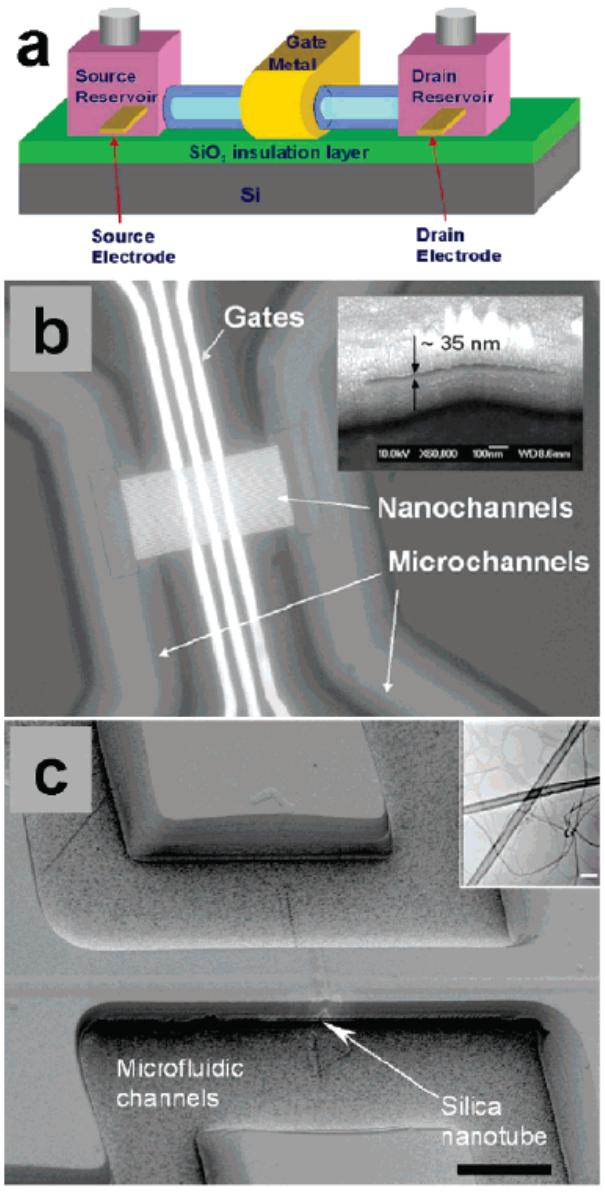

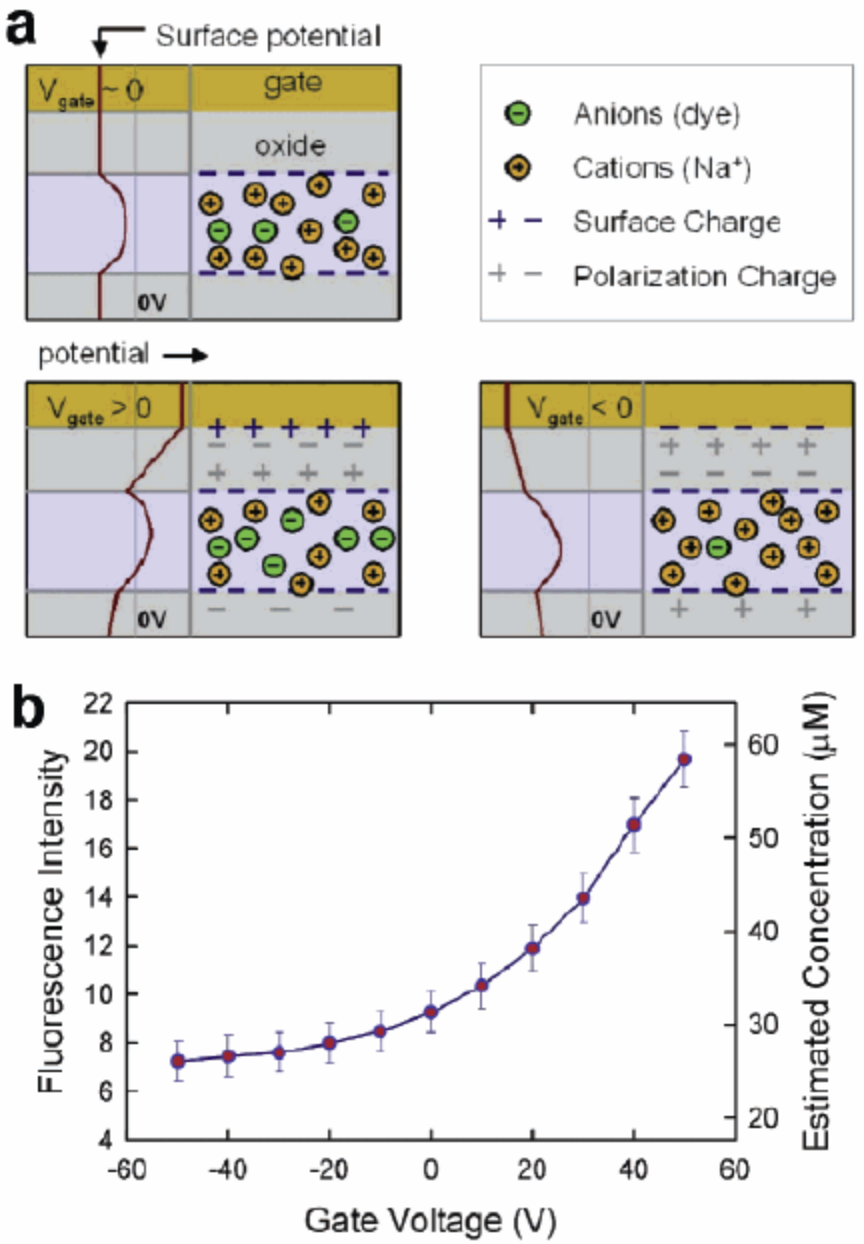

Karnik et al., Nano Letters 5(5):943-948, 2005.

Today's agenda

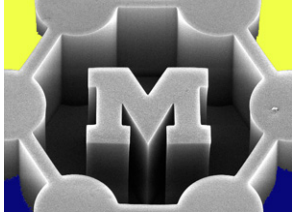

- Surface plasmon resonance (SPR): basic theory and effects of particle size and shape
- Example applications of SPR and surface-enhanced spectroscopy
- Plasmon-induced heating of metal nanoparticles

Today's readings

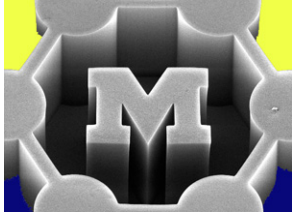

Nominal: (ctools)

- Kelly et al., "The optical properties of metal nanoparticles: the influence of size, shape, and dielectric environment"
- Murray and Barnes, "Plasmonic materials"
- Sriturvanich et al., "Flying plasmonic lens in the near field for plasmonic nanolithography"
- [illegible]d

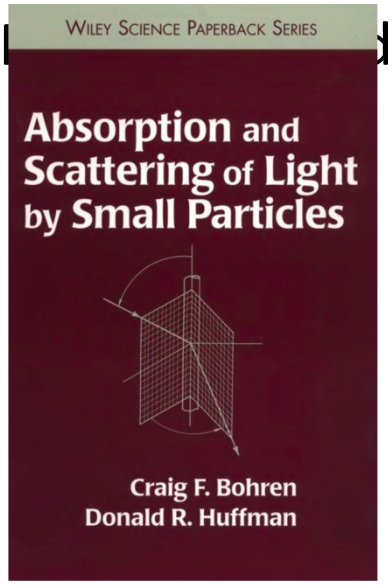

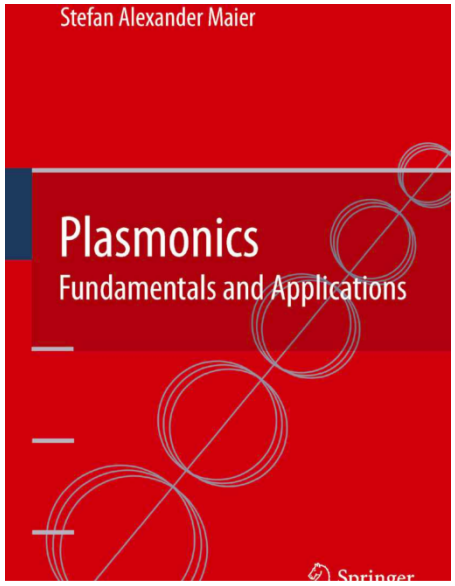

Surface plasmons: a hot topic

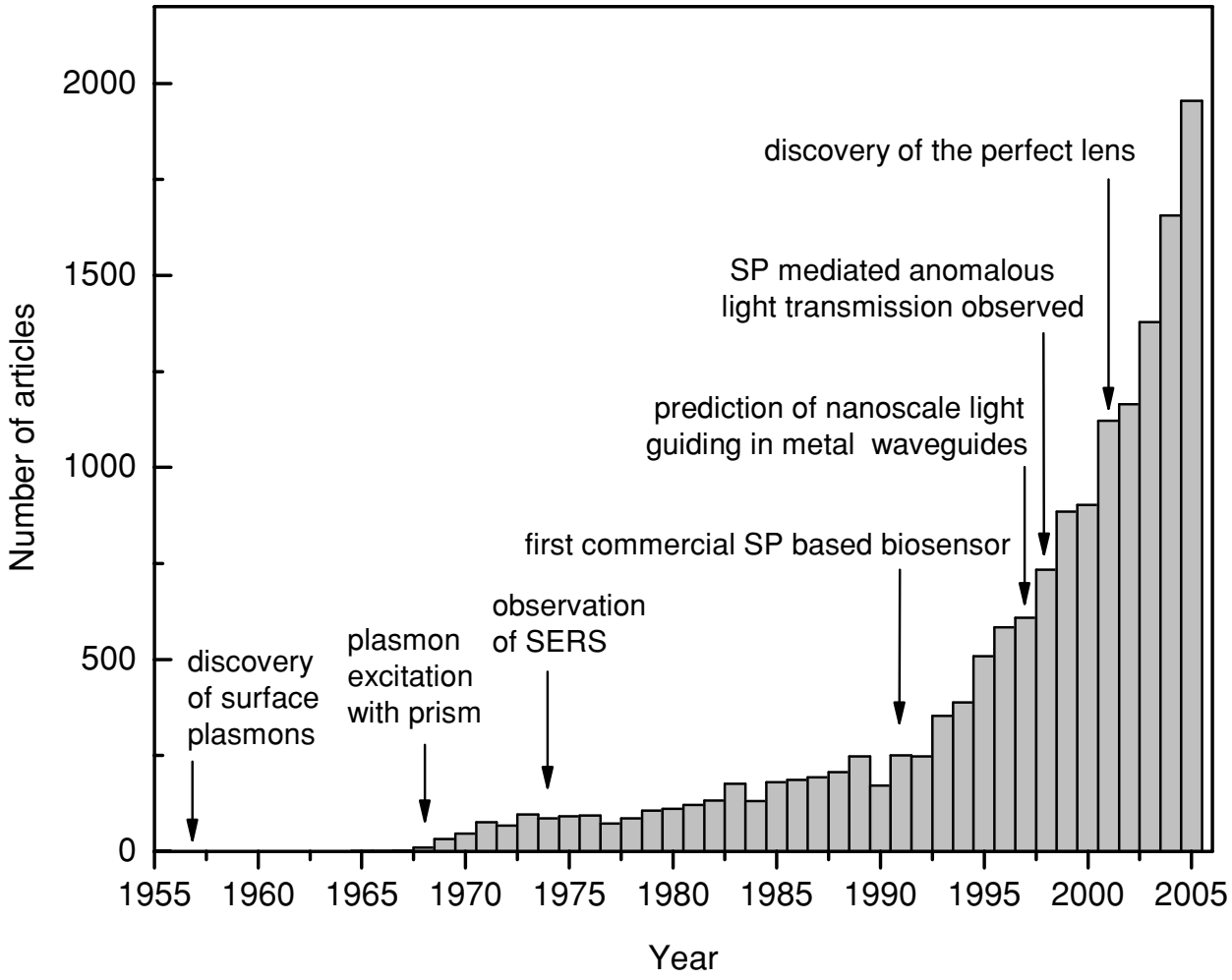

Figure 1.1. The growth of the field of metal nanophotonics is illustrated by the number of scientific articles published annually containing the phrase "surface plasmon" in either the title or abstract (based on data provided on www.sciencedirect.com).

Brongersma and Kik (Editors), Surface Plasmon Nanophotonics, Springer, 2007.

What is a plasmon?

- Plasmons are electromagnetic charge density waves

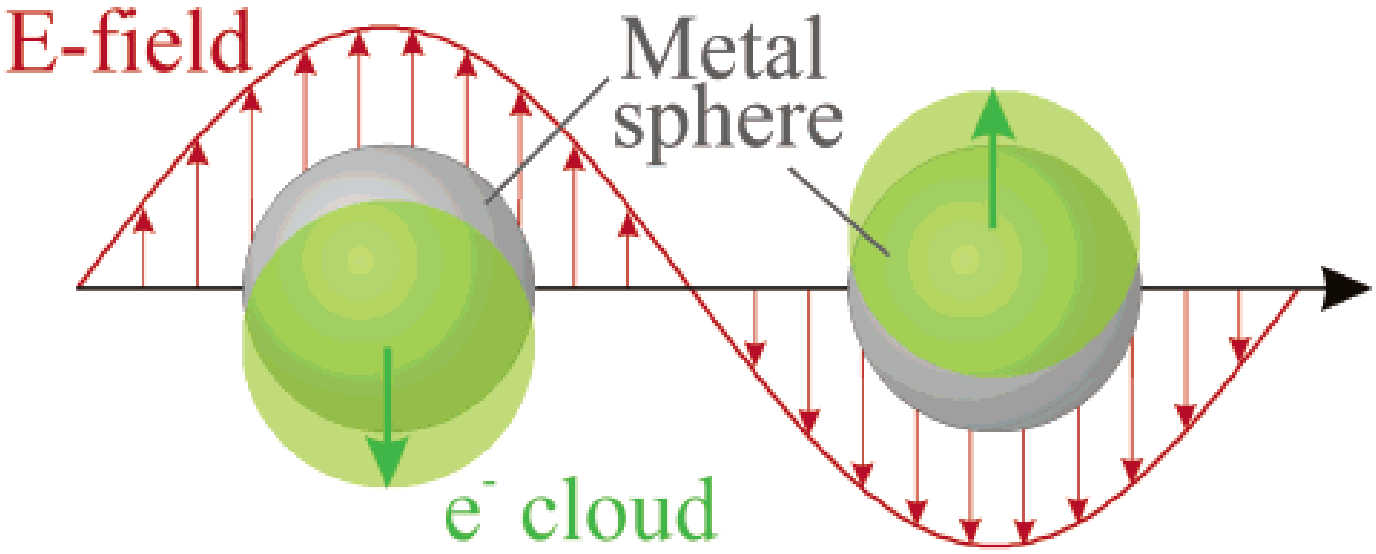

Figure 1. Schematic of plasmon oscillation for a sphere, showing the displacement of the conduction electron charge cloud relative to the nuclei.

- Surface plasmon resonance (SPR) occurs when a resonance of the charge density wave matches the frequency of the driving field

Kelly et al., J. Phys. Chem. B 107:668, 2003.

Visualizing SPR

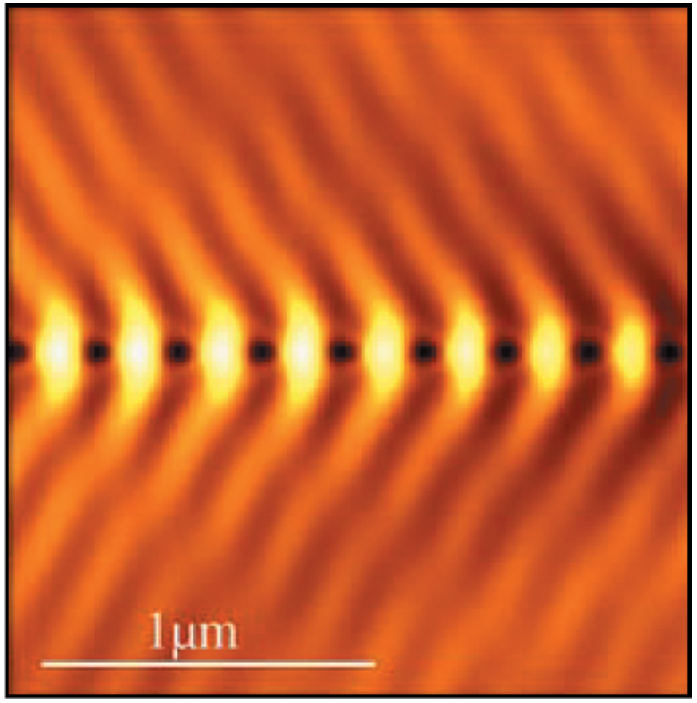

Optical near fields of metal nanoparticle chains with a grating constant of 400 nm. The chains are excited under total internal reflection from the right at 800 nm. The image was taken using a photon scanning tunneling microscope (STM). The circles indicate the nanoparticles.

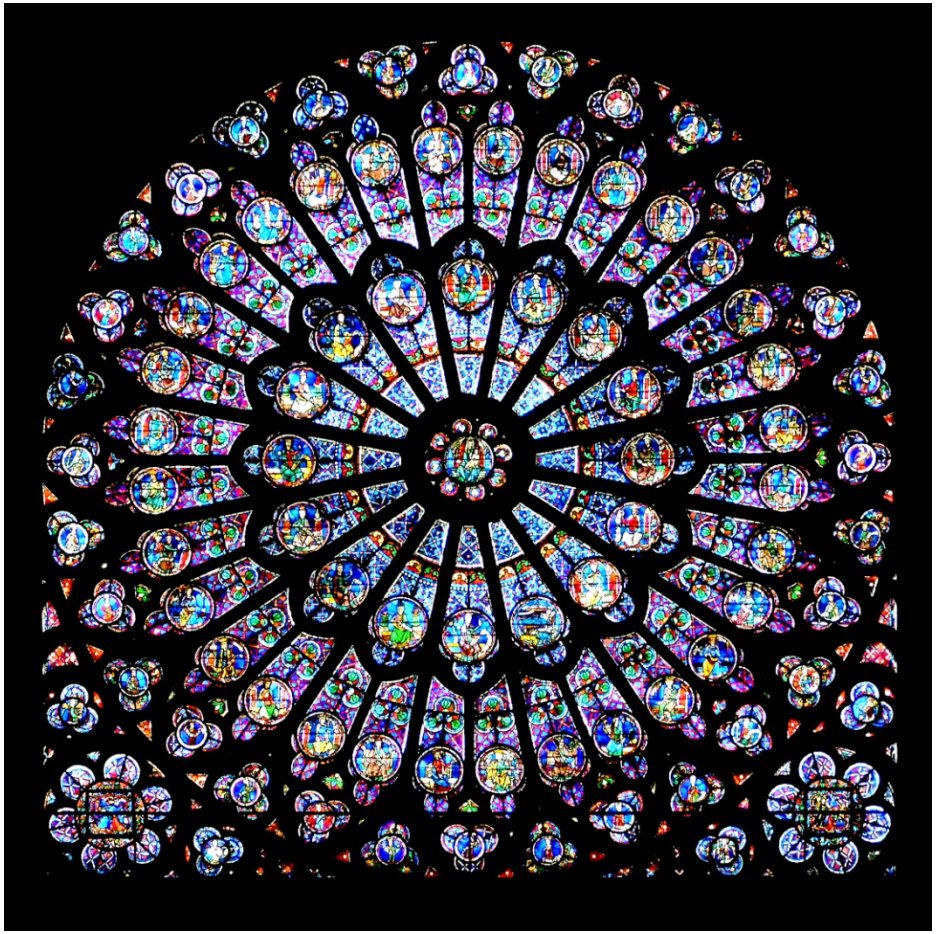

Brongersma and Kik (Editors), Surface Plasmon Nanophotonics, Springer, 2007.

Absorption and scattering

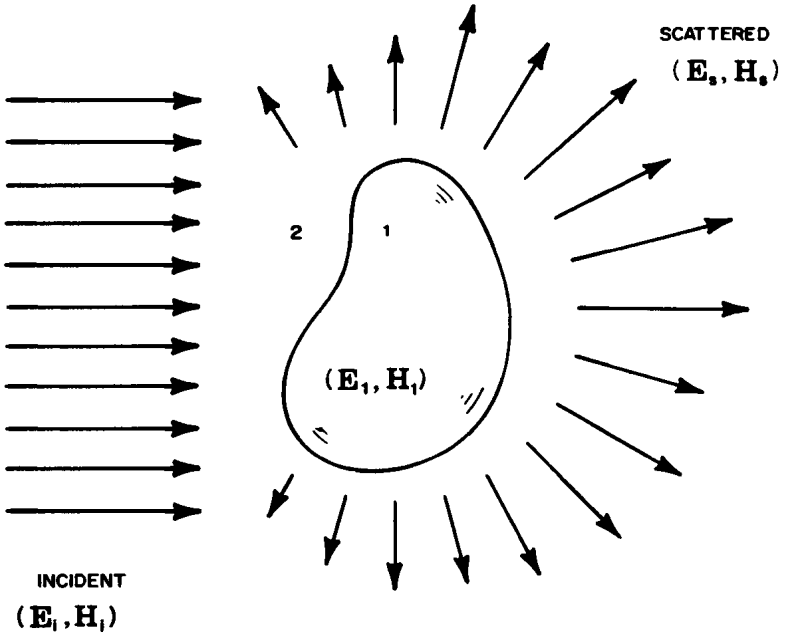

A particle with optical constants ε_p and μ_p is embedded in a medium with optical constants ε_m and μ_m, and illuminated by a plane wave, which generates an electric field E_1 and a magnetic field H_1 inside the particle. The particle radiates a scattered field in all directions, which leads, together with the applied fields, to an electric field E_2 and a magnetic field H_2 outside of the particle.

"Cross sections":

$$\sigma_{sca} = \frac{P_{sca}}{I_{inc}} \qquad \sigma_{abs} = \frac{P_{abs}}{I_{inc}} \qquad \sigma_{ext} = \frac{P_{ext}}{I_{inc}}$$

Scattering = secondary radiation

Conversion of radiation to another energy

Extinction = scattering + absorption

Bohren and Huffman, Absorption and scattering of light by small particles, Wiley and Sons, 1983.

Exact solution for a sphere: Mie theory

Maxwell's equations

$$\nabla \cdot \mathbf{E} = 0,$$

$$\nabla \cdot \mathbf{H} = 0,$$

$$\nabla \times \mathbf{E} = i\omega\mu\mathbf{H},$$

$$\nabla \times \mathbf{H} = -i\omega\varepsilon\mathbf{E},$$

$$\nabla \times (\nabla \times \mathbf{E}) = i\omega\mu\nabla \times \mathbf{H} = \omega^2\varepsilon\mu\mathbf{E},$$

$$\nabla \times (\nabla \times \mathbf{H}) = -i\omega\varepsilon\nabla \times \mathbf{E} = \omega^2\varepsilon\mu\mathbf{H},$$

$$\nabla \times (\nabla \times \mathbf{A}) = \nabla(\nabla \cdot \mathbf{A}) - \nabla \cdot (\nabla \mathbf{A})$$

Vector wave equation

$$\nabla^2\mathbf{E} + k^2\mathbf{E} = 0, \qquad \nabla^2\mathbf{H} + k^2\mathbf{H} = 0$$

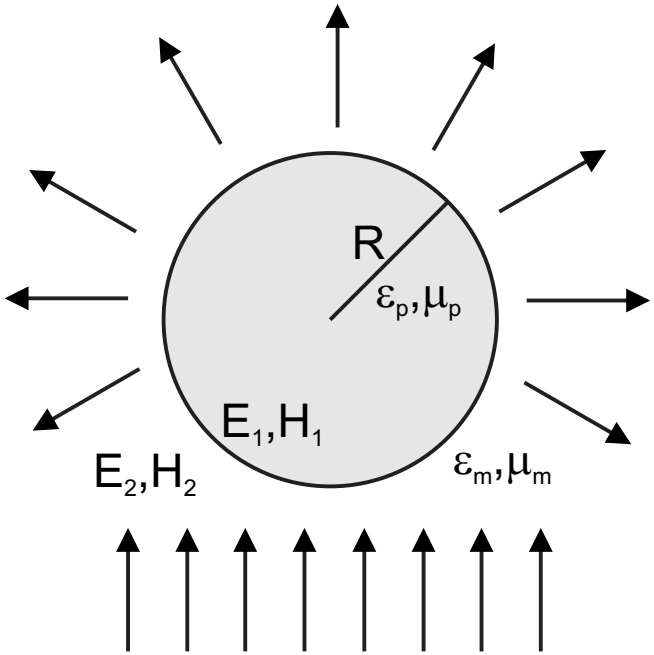

Bohren and Huffman, Absorption and scattering of light by small particles, Wiley and Sons, 1983.

Exact solution for a sphere: Mie theory

Boundary conditions:

$$[\mathbf{E}_2(\mathbf{x}) - \mathbf{E}_1(\mathbf{x})] \times \hat{\mathbf{n}} = 0$$
$$[\mathbf{H}_2(\mathbf{x}) - \mathbf{H}_1(\mathbf{x})] \times \hat{\mathbf{n}} = 0\,.$$

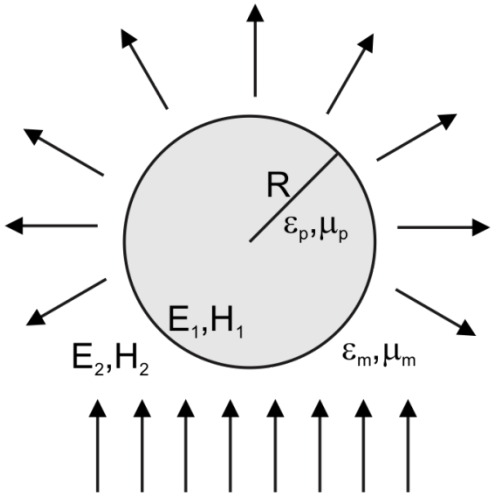

Cross sections:

$$\sigma_{sca} = \frac{2\pi}{\mathrm{k}^2}\sum_{n=1}^{\infty}(2n+1)\left(|a_n|^2+|b_n|^2\right)$$
$$\sigma_{ext} = \frac{2\pi}{\mathrm{k}^2}\mathrm{Re}\,(a_n+b_n)\ .$$

$$a_n = \frac{m\psi_n(mx)\psi_n'(x) - \psi_n(x)\psi_n'(mx)}{m\psi_n(mx)\xi_n'(x) - \xi_n(x)\psi_n'(mx)}$$
$$b_n = \frac{\psi_n(mx)\psi_n'(x) - m\psi_n(x)\psi_n'(mx)}{\psi_n(mx)\xi_n'(x) - m\xi_n(x)\psi_n'(mx)}$$

$$x = \mathrm{k}R$$
$$m = \sqrt{\epsilon_p/\epsilon_m}$$

Particles << wavelength: the Rayleigh limit

$$\sigma_{abs} \approx \sigma_{ext} = \mathrm{k}\,\mathrm{Im}(\alpha) = 4\pi\,\mathrm{k}\,R^3\,\mathrm{Im}\left(\frac{\epsilon_p-\epsilon_m}{\epsilon_p+2\epsilon_m}\right)$$
$$\sigma_{sca} = \frac{\mathrm{k}^4}{6\pi}|\alpha|^2 = 8\pi\,\mathrm{k}^4\,R^6\left|\frac{\epsilon_p-\epsilon_m}{\epsilon_p+2\epsilon_m}\right|^2$$

Exact solution for a sphere: Mie theory

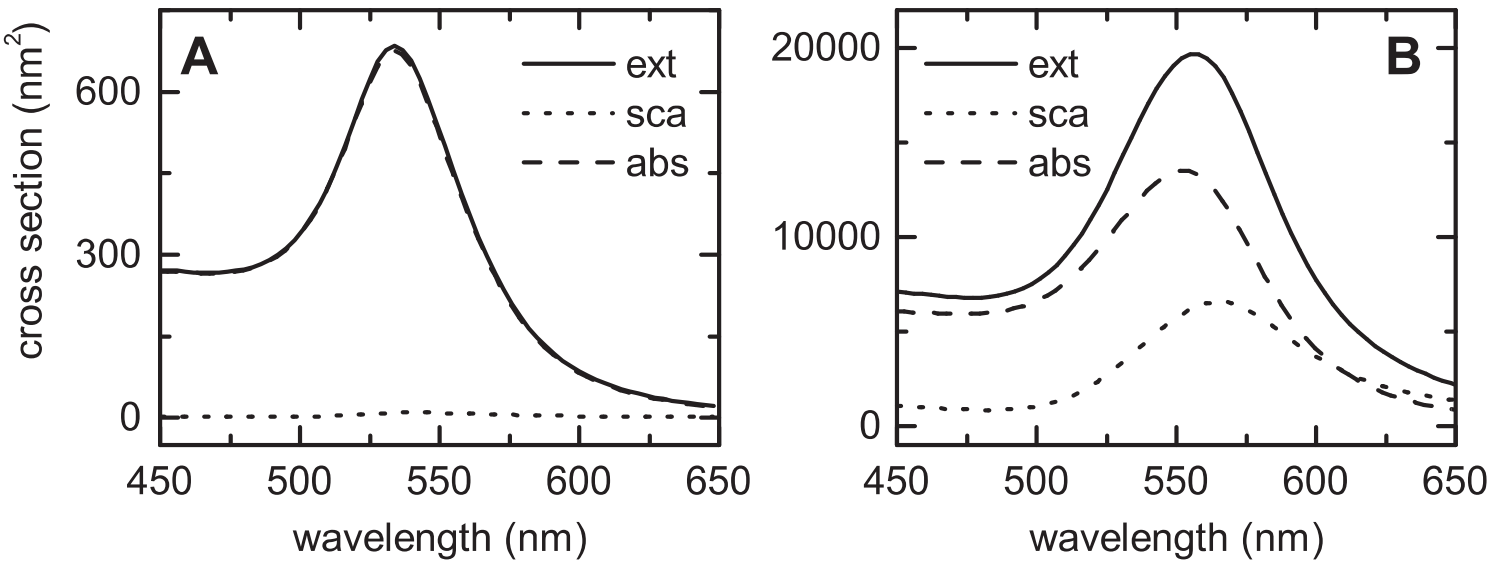

Figure 1.3: Extinction, scattering and absorption spectra of a particle with a radius of 10 nm (A) and a radius of 30 nm (B). In both cases, the refractive index of the environment is 1.5. Note that for the 10-nm particle, the scattering cross section nearly vanishes, and as a result of that, the absorption and extinction cross sections are approximately equal.

Meindert Alexander van Dijk, Nonlinear-optical studies of single gold nanoparticles, Ph.D. Thesis, Leiden University, 2007.

Effect of size and surroundings

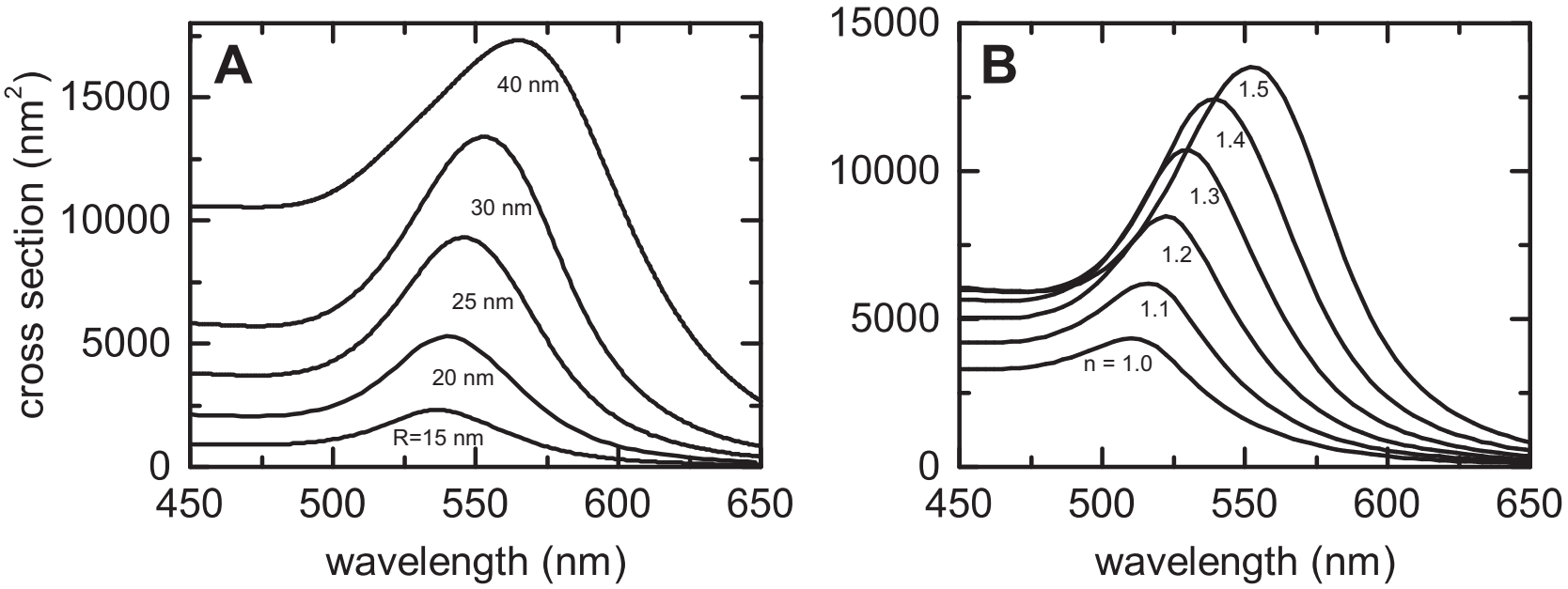

Figure 1.4: Absorption spectra for increasing radius with $n_m = 1.5$ (A), and for increasing refractive index with $R = 30$ nm (B).

Meindert Alexander van Dijk, Nonlinear-optical studies of single gold nanoparticles, Ph.D. Thesis, Leiden University, 2007.

Normal modes: dipole and quadrupole

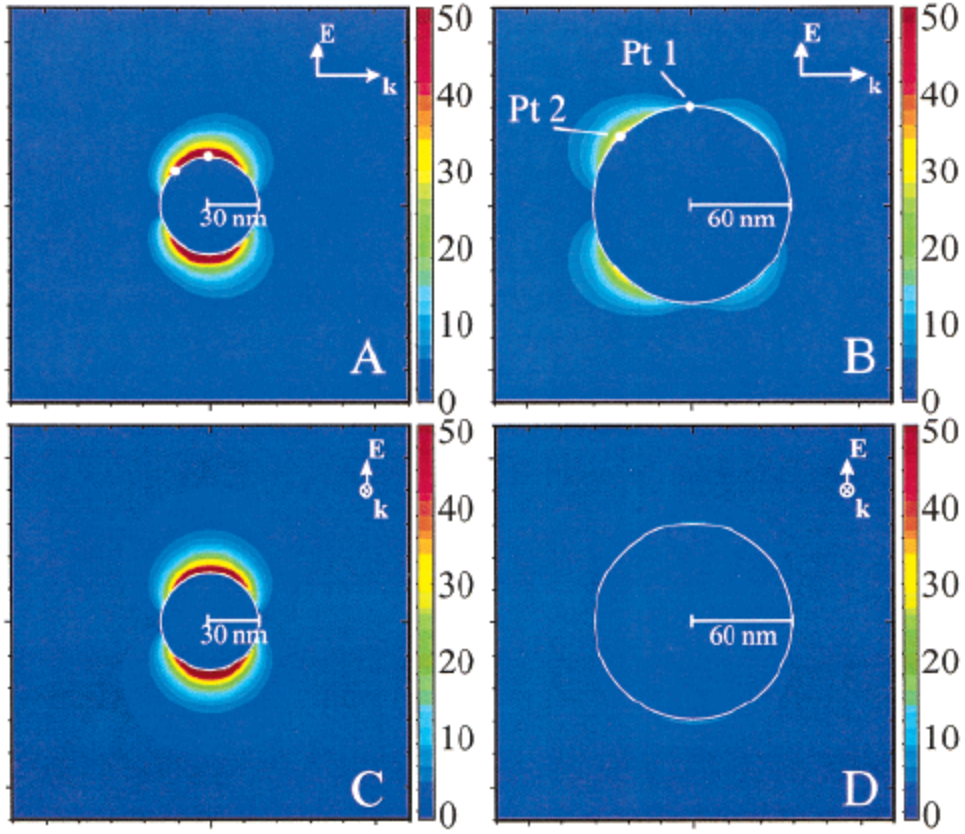

Figure 3. E-field contours for radius 30 and 60 nm Ag spheres in a vacuum. Two cross-sections are depicted for each sphere. (a, b) The plane containing the propagation and polarization axes and (c, d) the plane perpendicular to the propagation axis. The 30 nm sphere refers to 369 nm light, the main extinction peak for this size, whereas the larger sphere is for 358 nm light, the quadrupole peak for this size. Labeled points 1 and 2 illustrate locations for Figure 4.

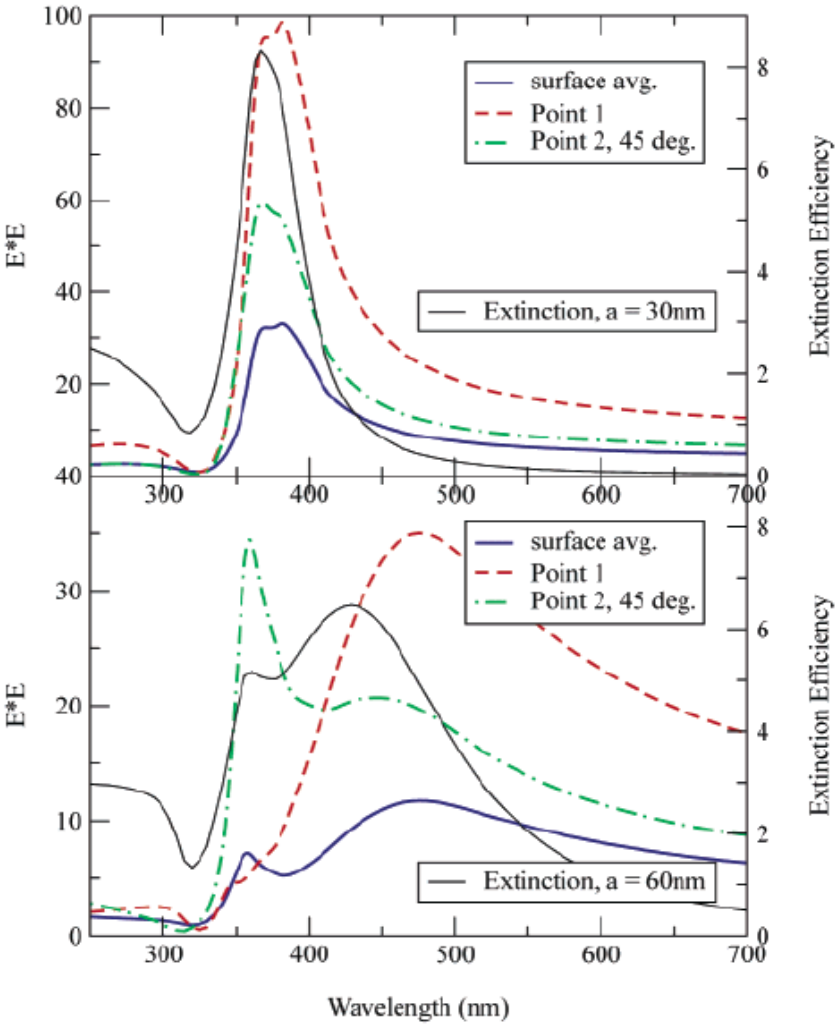

Kelly et al., J. Phys. Chem. B 107:668, 2003.

Near fields at planar surfaces

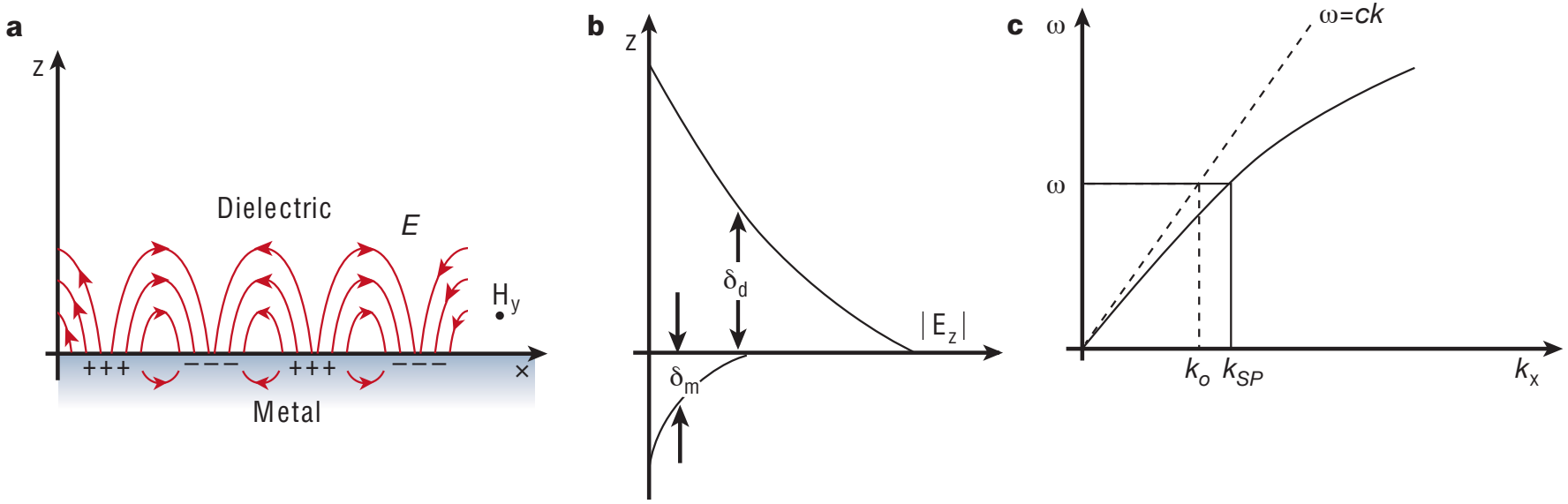

Rough surfaces:

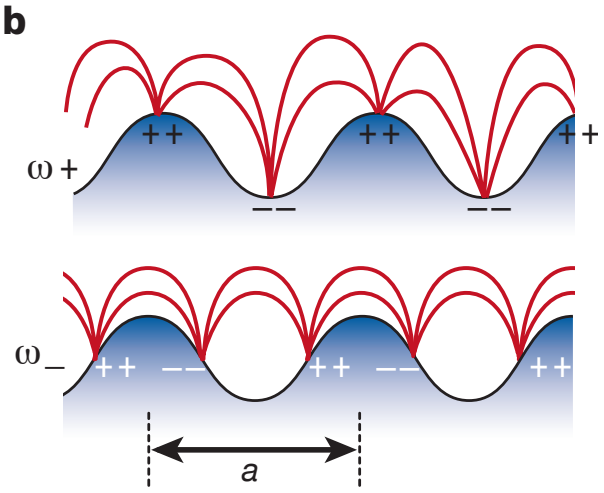

Barnes et al., Nature 424:824-830, 2003.

The dielectric function of an electron gas

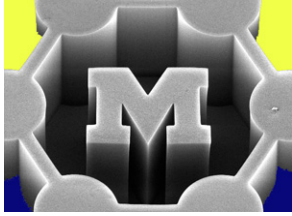

$\vec{D}$ = dielectric displacement

= $\varepsilon_0 \vec{E} + \vec{P}$ — electric dipole per unit volume

$\rightarrow$ $\vec{D} = \varepsilon_0 \varepsilon \vec{E}$

ε — dielectric constant (relative permittivity)

The Drude model for free electrons

$$m\frac{d^2\vec{x}}{dt^2} + m\gamma\frac{d\vec{x}}{dt} = -e\vec{E}$$

$$\vec{E}(t) = \vec{E}_0 e^{-i\omega t}$$

$\gamma = \frac{1}{\tau}$ ← relaxation time

(= collision frequency)

harmonic dependance:

$$\vec{x}(t) = \vec{x}_0 e^{-i\omega t}$$

$$= \frac{e}{m(\omega^2 + i\gamma\omega)}\vec{E}(t)$$

Solve for dielectric constant

$$\vec{P} = -ne\vec{x}$$

$$= \frac{-ne^2}{m(\omega^2 + i\gamma\omega)}\vec{E}$$

$$\Rightarrow \vec{D} = \varepsilon_0\left(1 - \frac{\omega_p^2}{\omega^2 + i\gamma\omega}\right)\vec{E}$$

$$\varepsilon(\omega)$$

$\omega_p \equiv$ 'plasma Frequency'

$$= \frac{ne^2}{\varepsilon_0 m}$$

Solve for dielectric constant

$$\varepsilon(\omega) = \varepsilon_1(\omega) + i\,\varepsilon_2(\omega)$$

$$\varepsilon_1 = 1 - \frac{\omega_p^2 \tau^2}{1 + \omega^2 \tau^2}$$

$$\varepsilon_2 = \frac{\omega_p^2 \tau}{\omega(1 + \omega^2 \tau^2)}$$

$$\varepsilon = N^2 \qquad N = n + iK$$

Compared with real data

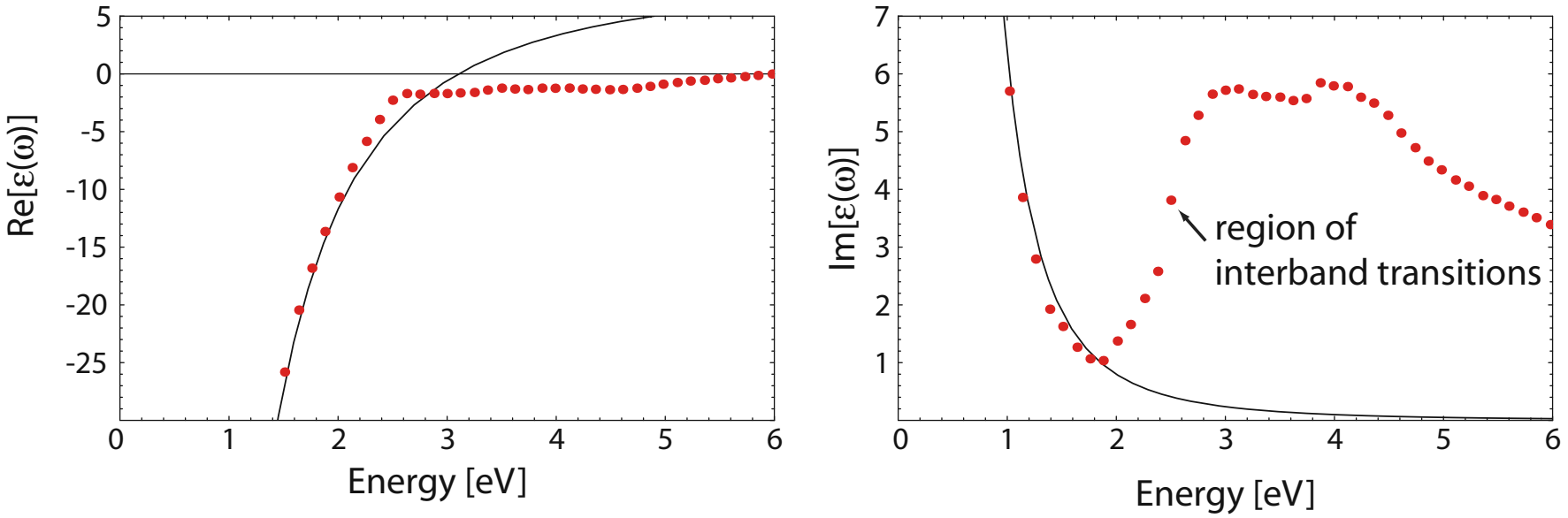

Figure 1.1. Dielectric function $\varepsilon(\omega)$ (1.27) of the free electron gas (solid line) fitted to the literature values of the dielectric data for gold [Johnson and Christy, 1972] (dots). Interband transitions limit the validity of this model at visible and higher frequencies.

Maier, Plasmonics: fundamentals and applications, Springer, 2007.

The importance of the plasma frequency

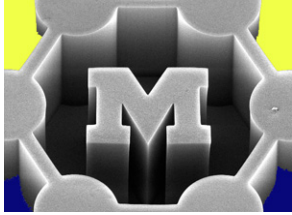

Geometry	Resonance condition	Resonance frequency
Bulk metal	$\varepsilon_1(\omega) = 0$	$\omega_1 = \omega_p$
Planar surface	$\varepsilon_1(\omega) = -1$	$\omega_1 = \omega_p/\sqrt{2}$
Sphere (dipole mode)	$\varepsilon_1(\omega) = -2$	$\omega_1 = \omega_p/\sqrt{3}$

Kreibig and Vollmer, Optical properties of metal clusters, Springer, 1995 pp. 14 – 25.

The Lorentz model

9.1 THE LORENTZ MODEL

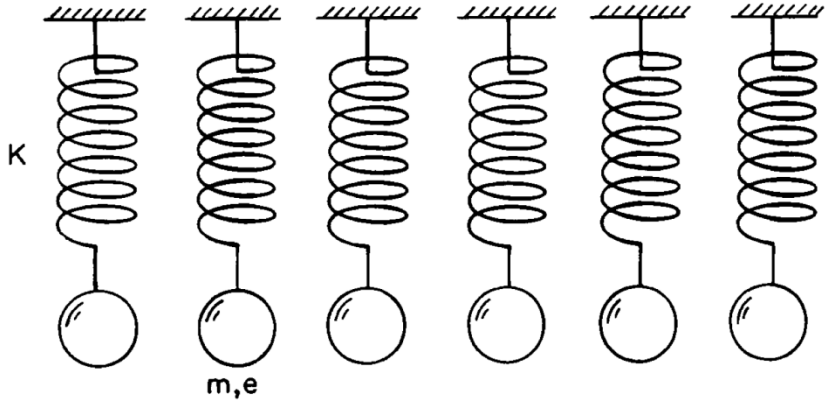

Figure 9.1 The Lorentz model of matter.

$$m\ddot{\mathbf{x}} + b\dot{\mathbf{x}} + K\mathbf{x} = e\mathbf{E}_{\text{local}}$$

$$\mathbf{x} = \frac{(e/m)\mathbf{E}}{\omega_0^2 - \omega^2 - i\gamma\omega}$$

$$\mathbf{P} = \frac{\omega_p^2}{\omega_0^2 - \omega^2 - i\gamma\omega}\varepsilon_0\mathbf{E},$$

$\omega_0^2 = K/m$ and $\gamma = b/m$.

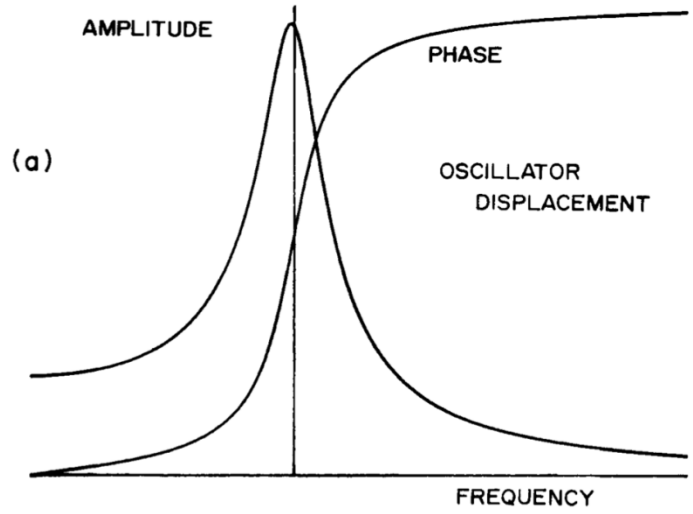

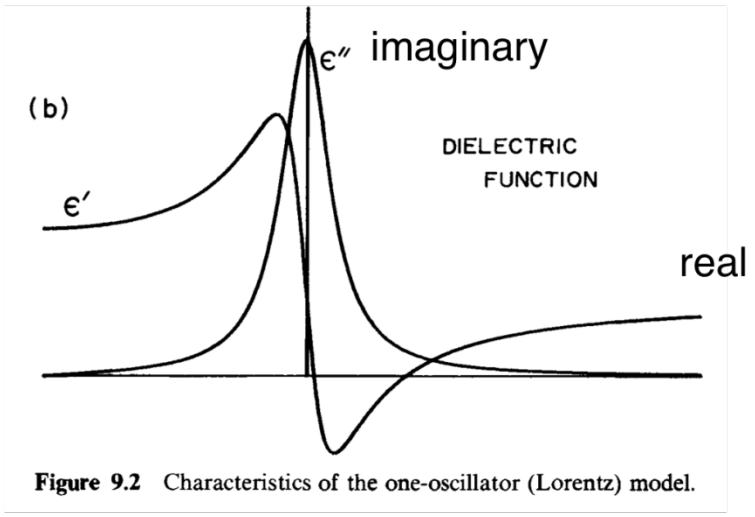

Figure 9.2 Characteristics of the one-oscillator (Lorentz) model.

Nanosphere lithography

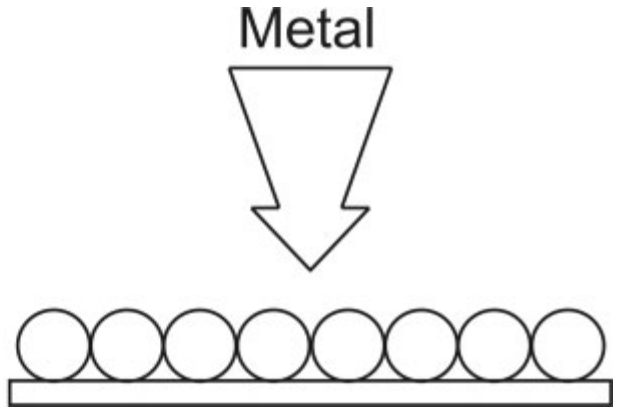

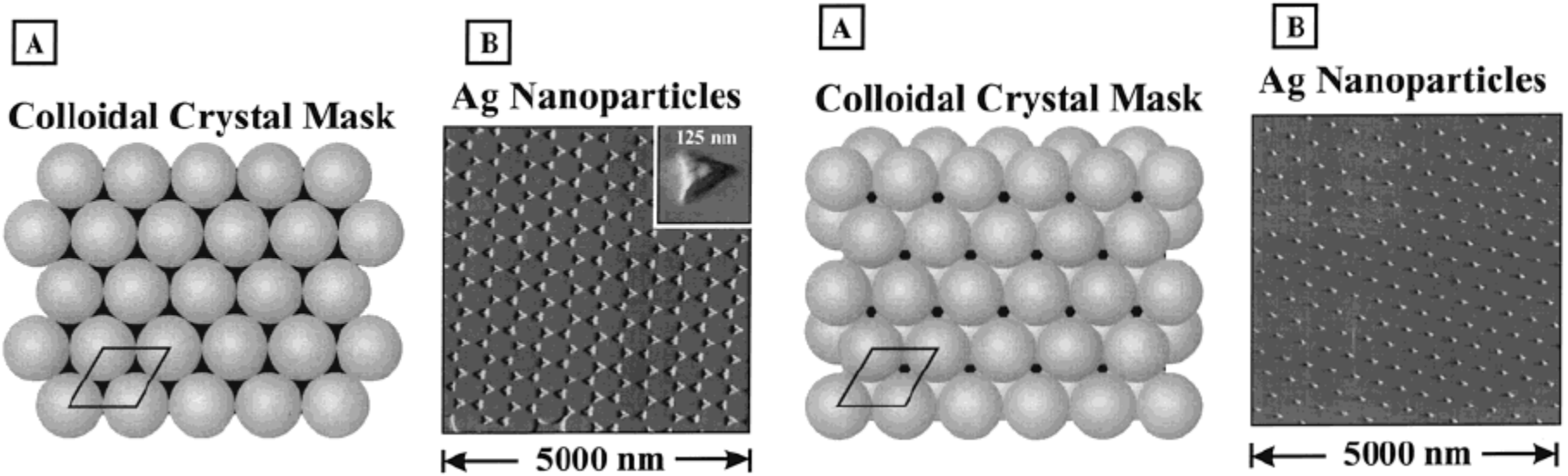

Murray and Barnes, Advanced Materials 19:3771-3782, 2007; van Duyne et al., Northwestern

SPR tuning via nanosphere lithography

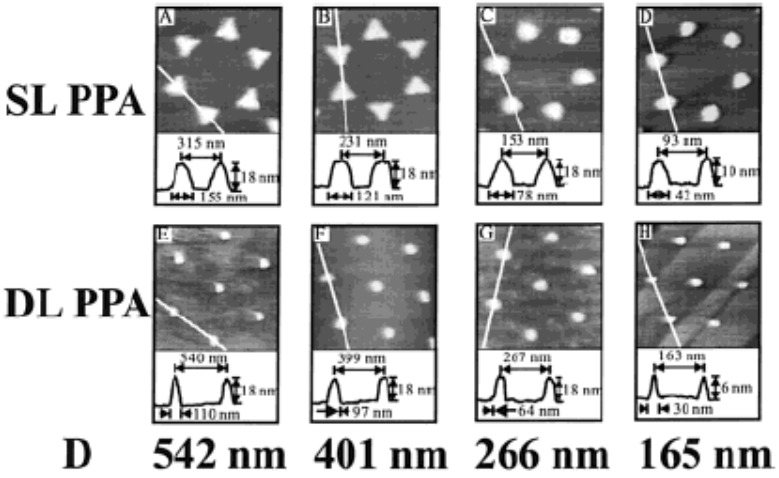

Figure 10. AFM images and line scans of representative Ag nanoparticle arrays on mica substrates. The line scan values reported here have not been deconvoluted for tip broadening effects. (A) 870 nm × 870 nm image, D = 542 nm, d_m = 18 nm; (B) 610 nm × 610 nm image, D = 401 nm, d_m = 18 nm; (C) 420 nm × 420 nm image, D = 264 nm, d_m = 18 nm; (D) 260 nm × 260 nm image, D = 165 nm, d_m = 14 nm; (E) 1200 nm × 1200 nm image, D = 542 nm, d_m = 18 nm; (F) 1000 nm × 1000 nm image, D = 401 nm, d_m = 18 nm; (G) 670 nm × 670 nm image, D = 264 nm, d_m = 18 nm; (H) 410 nm × 410 nm image, D = 165 nm, d_m = 0.5 nm.

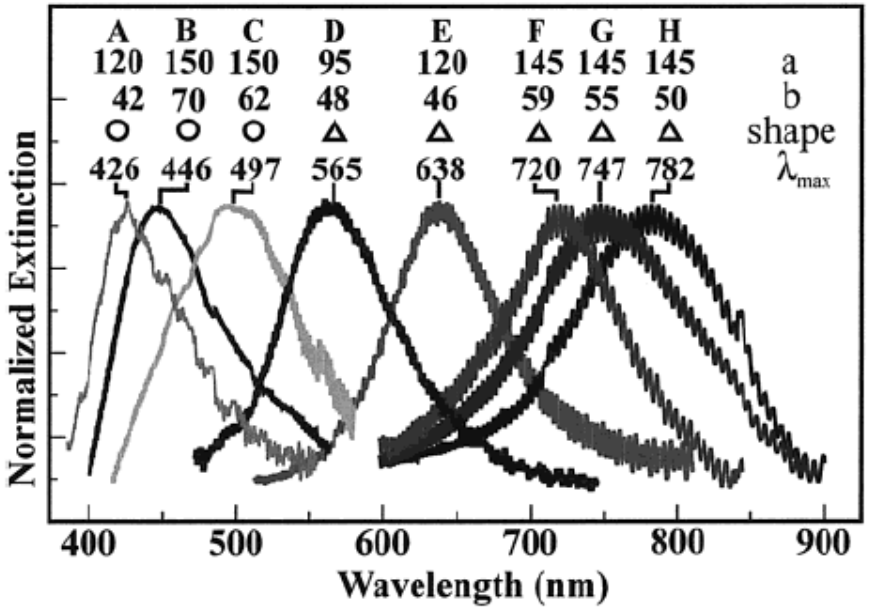

Figure 11. UV−visible extinction spectra of Ag SL PPA on mica substrates. Reported spectra are raw, unfiltered data. The oscillatory signal superimposed on the LSPR spectrum seen in the data is due to interference of the probe beam between the front and back faces of the mica.

Haynes and Van Duyne, J. Physical Chemistry B 105:5599:5611, 2001.

Effect of shape (Ag “nanoprism”)

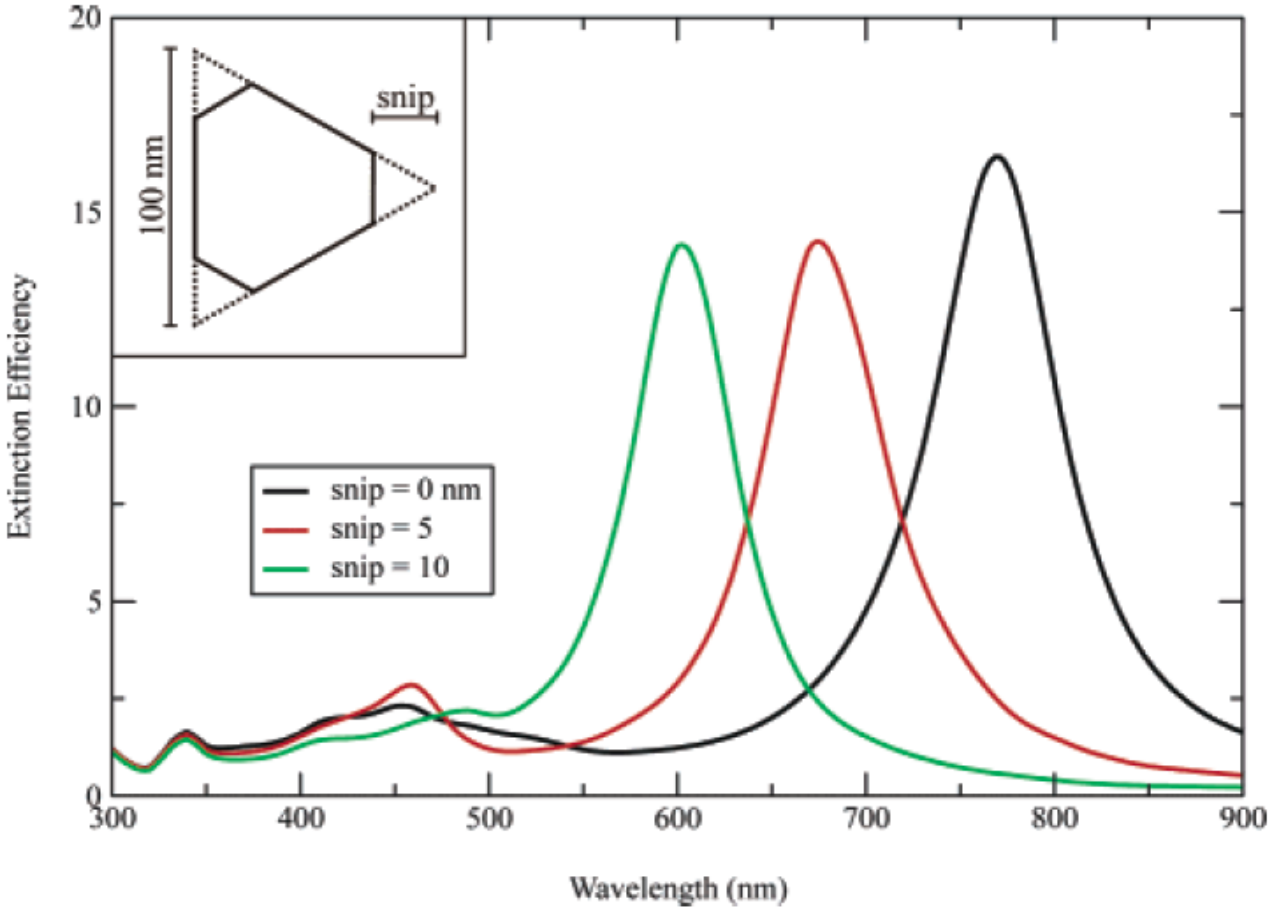

Kelly et al., J. Phys. Chem. B 107:668, 2003.

Effect of environment (dielectric)

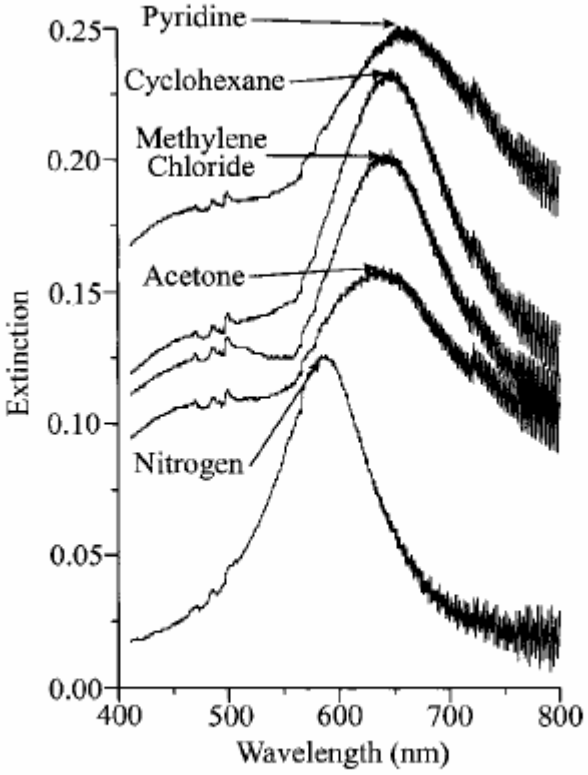

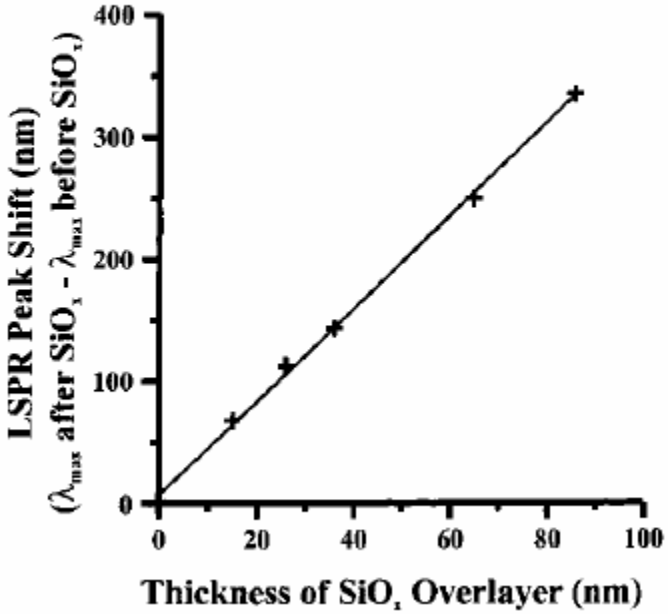

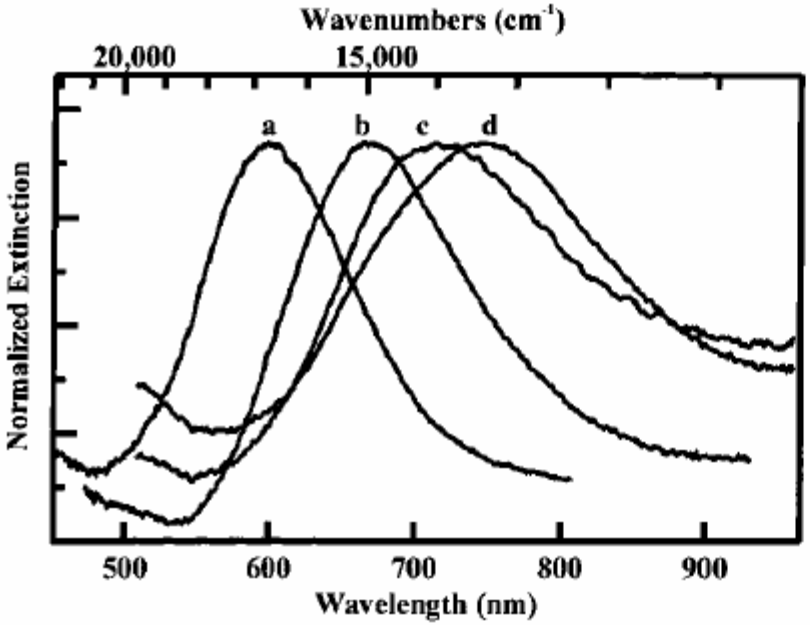

Van Duyne et al.

Effect of particle coupling

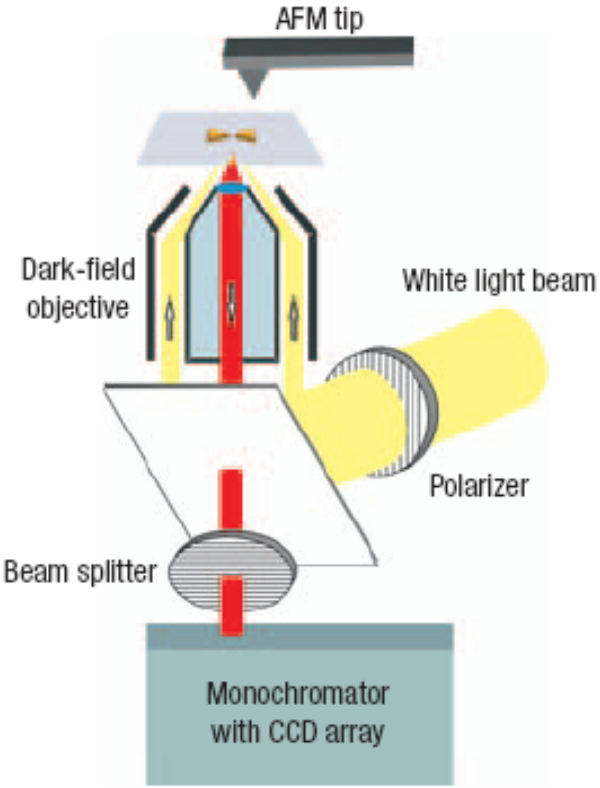

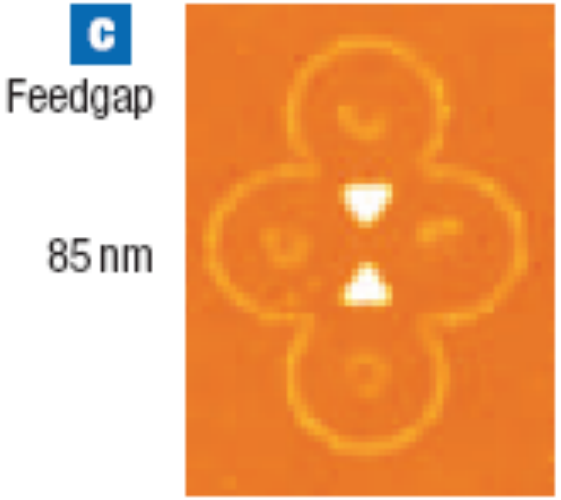

Figure 1 Nano-optomechanical set-up. Schematic drawing of the experimental set-up (not to scale) consisting of an AFM and dark-field scattering spectroscopy system.

Merlein et al., Nature Photonics 2:230-233, 2008.

Effect of particle coupling

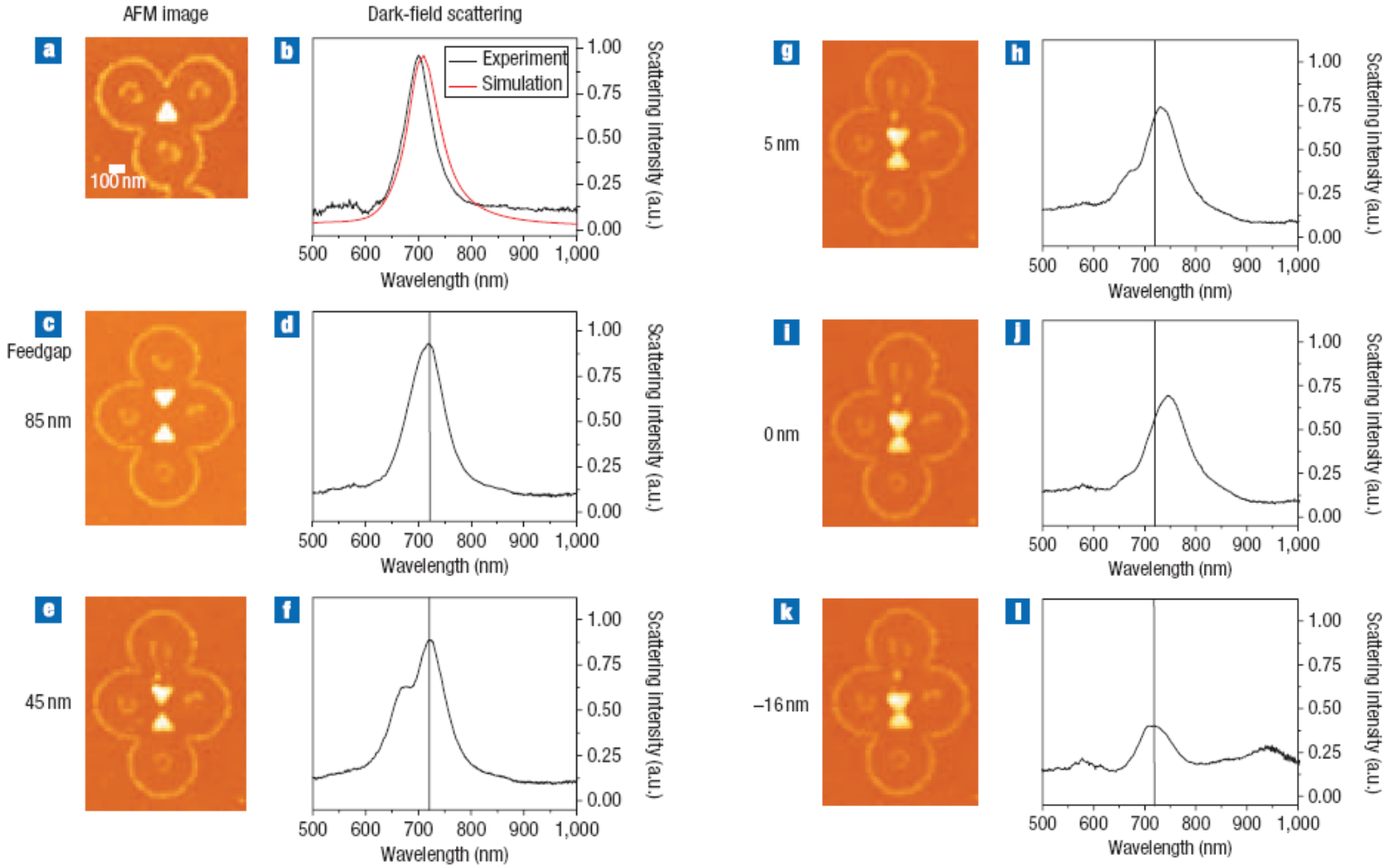

Merlein et al., Nature Photonics 2:230-233, 2008.

Effect of particle coupling

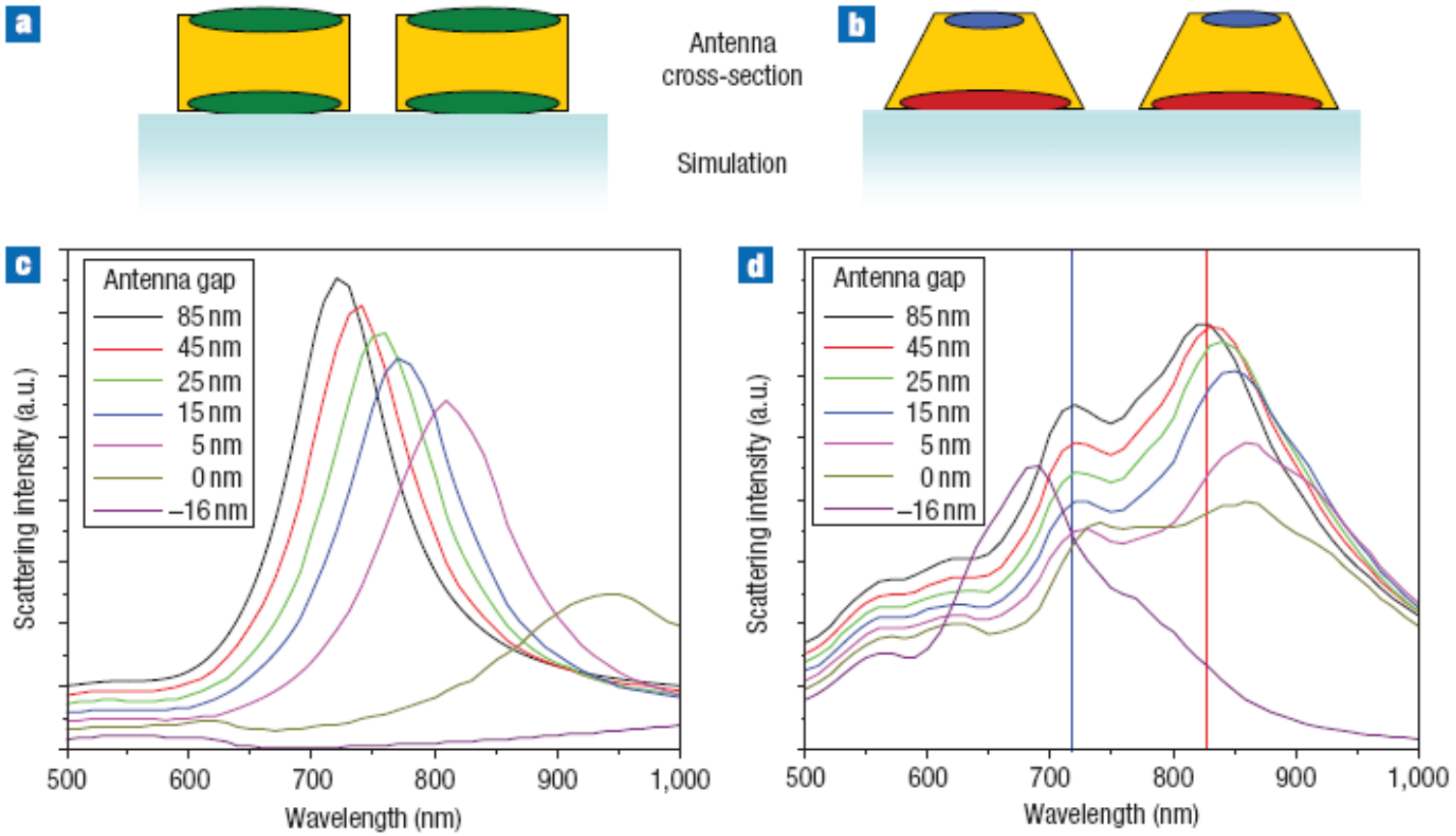

Figure 3 Calculated backscattering spectra depending on the three-dimensional antenna shape. **a**,**b**, Schematic drawings of a nanoantenna cross-section for vertical (**a**) and tilted (**b**) sidewalls of the antenna arms. The glass/gold surface plasmon is depicted in red, the gold/air surface plasmon in blue. **c**,**d**, Calculated backscattering spectra of the gold bow-tie nanoantenna (side length, 128 nm; thickness, 32 nm) at different gap sizes assuming vertical sidewalls (**c**) and tilted sidewalls (dihedral angle base–sidewall, 54°) (**d**). The excitation and detection polarizations are set in the direction of the long antenna axis.

Merlein et al., Nature Photonics 2:230-233, 2008.

A plasmon ruler

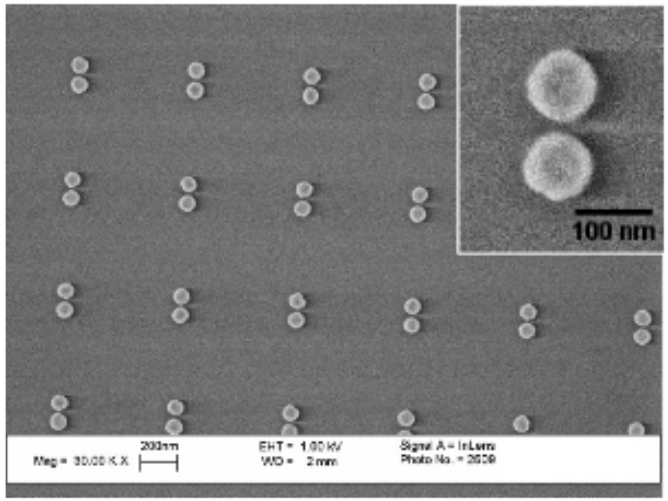

- Closer = red-shift
- Polarization is important

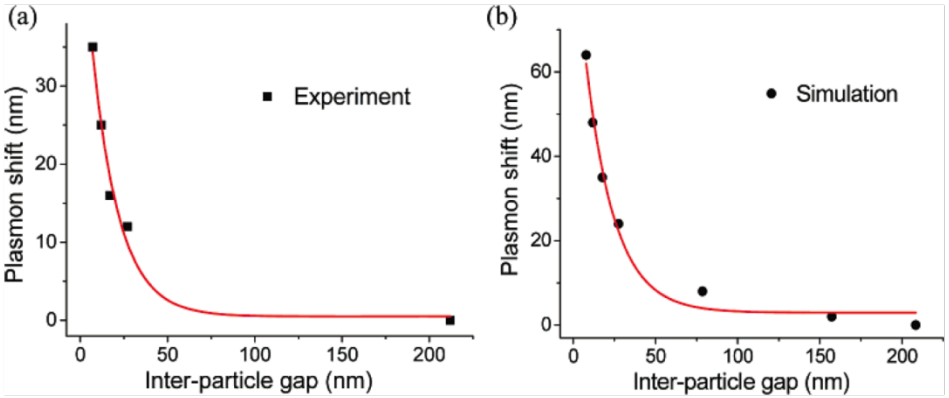

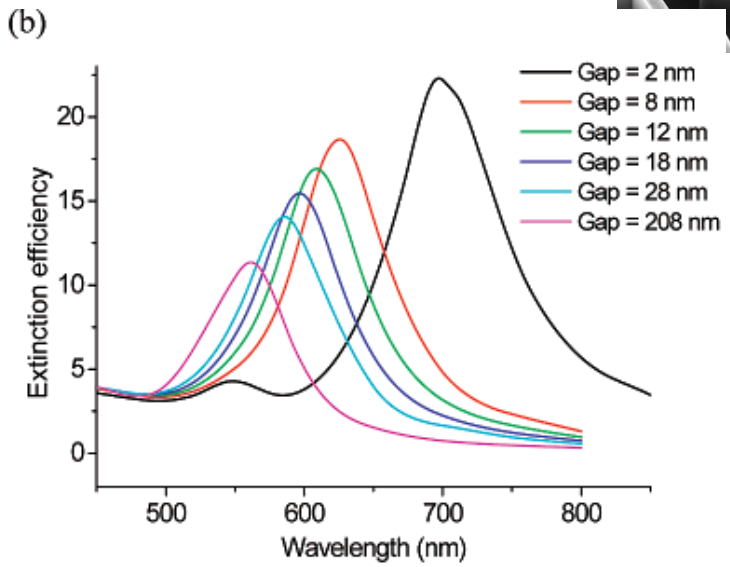

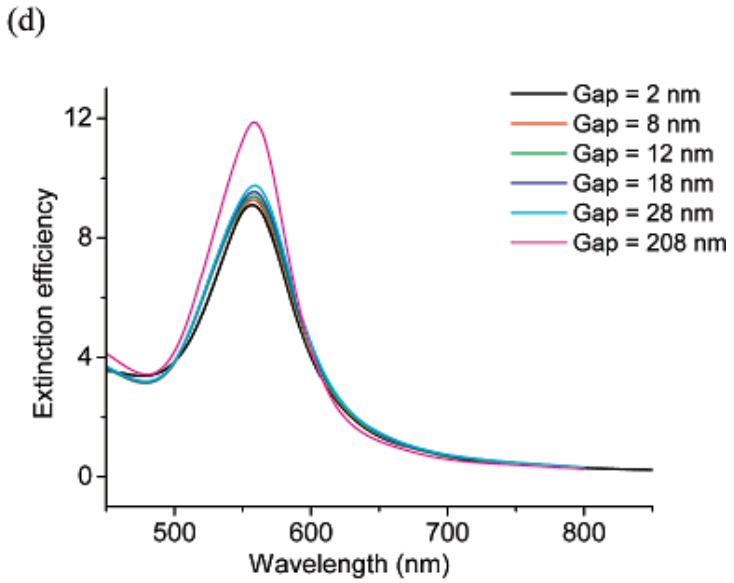

Nano Lett., Vol. 7, No. 7, **2007**

Single molecule Raman spectroscopy (SERS) → hotspots!

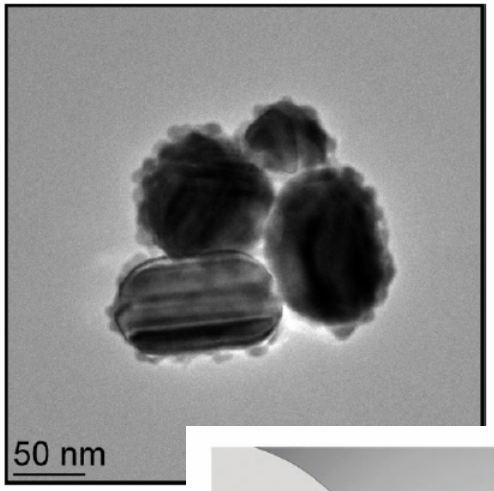

Figure 4. High-resolution
SMSERS aggregate. Spectr

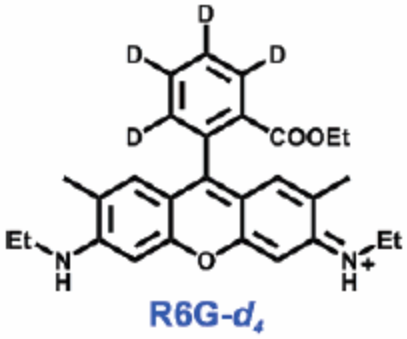

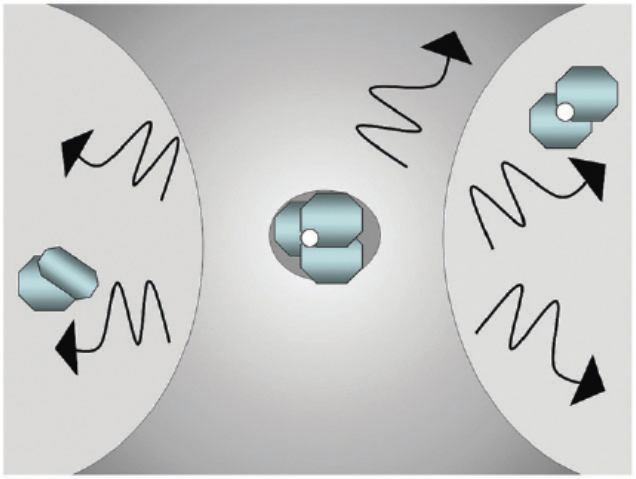

Fig. 4 The combination of small probe area and dilute concentration of the target molecule is necessary for SMD experiments.

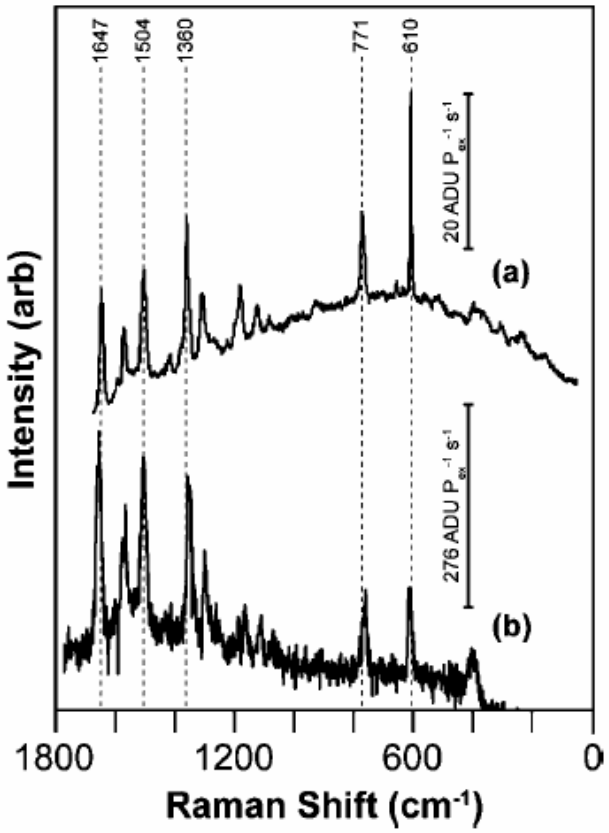

Figure 2. Surface-enhanced Raman spectra of R6G on silver obtained using 532-nm excitation. (a) Ensemble-averaged surface-enhanced resonance Raman obtained on AgIF (P_{ex} = 2.0 kW·cm^{-2}, t_{ac} = 0.1 s) and (b) single-molecule surface-enhanced resonance Raman spectrum obtained on colloidal Ag aggregate (P_{ex} = 0.050 W·cm^{-2}, t_{ac} = 30 s).

Van Duyne , et al.; Aroca, et al.

Biomolecular sensing

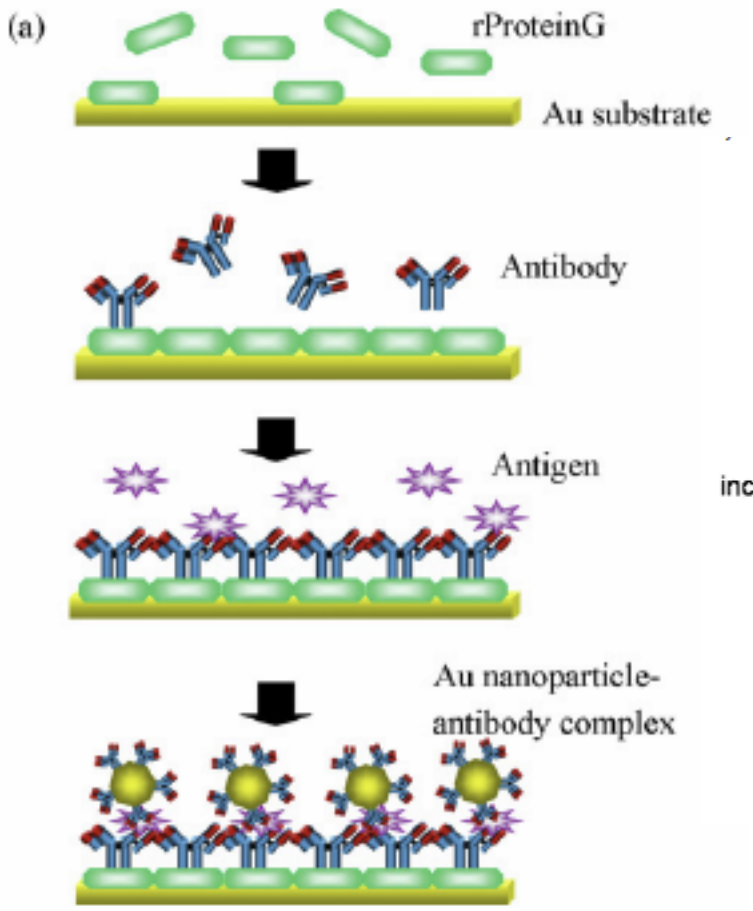

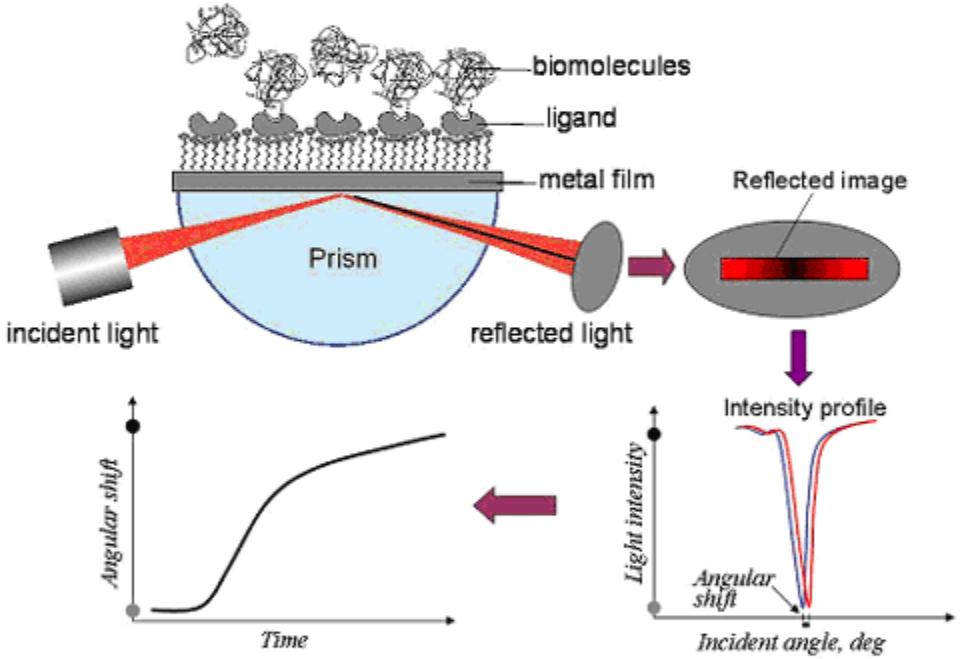

Biacore: commercial SPR instruments
http://www.biacore.com/lifesciences/technology/introduction/data_interaction/index.html
http://www.biosensingusa.com/Application101.html

Choi et al., Collids and Surfaces, A 313-314:655-659 2008.

Biomolecular sensing

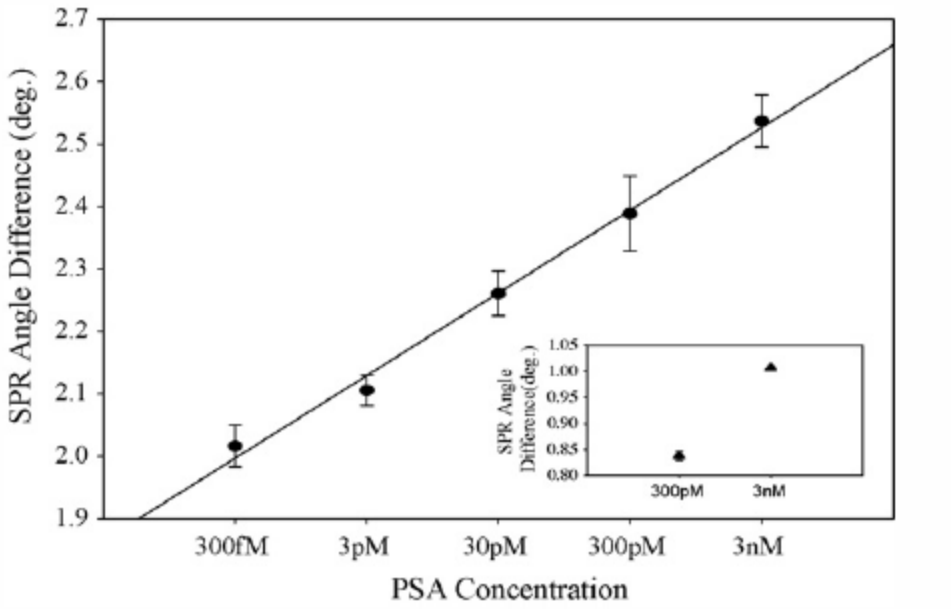

Fig. 5. Plot of SPR angle shift vs. antigen (prostate-specific antigen, PSA) concentration; (●) variation of angle difference when the Au nanoparticle; and (▲) variation of angle difference which was measured without label.

Choi et al., Collids and Surfaces, A 313-314:655-659 2008.

Biomolecular sensing

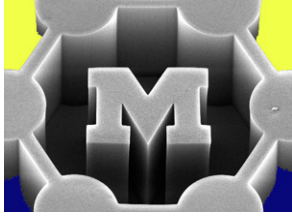

Table 4. Examples of biosensor formats applied to PSA detection

Signal transduction	Assay format and/or nanostructure used	Lowest detection limit	Sample volume required (μl)	Assay time (mins)	Refs
Time-resolved fluorescence	Europium (III) chelate-dyed polystyrene nanoparticles	0.21 ng/ml	20	~240	[48]
	Silica-coated terbium (III) fluorescent nanoparticles	7.0 pg/ml	45	>180	[18]
	Terbium complex-doped zirconia nanoparticles	0.4 ng/ml	45	>180	[20]
	Europium(III) nanoparticle labels and streptavidin–biotin technology	0.83 pg/ml	5	>150	[19]
SERS	Gold nanoparticles	1.0 pg/ml	40	~550	[21]
Real-time Immuno-PCR	Sandwich assay with DNA label on detection antibody	0.2 pg/ml[a]	5.5	>150	[24]
Immuno-RCA	Sandwich assay with DNA label on detection antibody	0.1 pg/ml	10	~180	[25]
Biobarcode	Gold nanoparticles	1.0 fg/ml[b]	10	80	[26]
		1.0–10.0 fg/ml	250	~210	[27]
Enzyme and/or impedance	Lateral flow immunostrip containing an electrochemical transducer	3.0 ng/ml	11	10–30	[29]
Enzyme and/or amperometric	Sandwich immunoassay on three-electrode system	0.25 ng/ml	10	60	[31]
Surface plasmon resonance	Commercial SPR biochip with signal enhancement using a sandwich-assay format	18.1 ng/ml	100	14	[35]
		1.0 ng/ml	130	6.5	[34]
		0.15 ng/ml	NS	NS	[49]
Surface plasmon fluorescence spectroscopy	Sandwich-immunoassay format on commercial SPR biochip	3 pg/ml	500	45	[50]
Electrical	Resonance frequency shift in a nanomechanical microcantilever	10 pg/ml	NS	NS	[36]
		100 ng/ml	20	60	[37]
	Surface stress bending of piezoresistive self-sensing microcantilevers	10 ng/ml	NS	10	[38]
	Conductance change in silicon nanowire sensor chip	100 fg/ml	NS	30	[40]

[a]Sensitivity reported by authors as 4.8×10^5 PSA molecules, converted to pg/ml for consistency; [b]sensitivity reported as 30 aM, converted to fg/ml for consistency.
Abbreviation: NS, not specified by authors.

Healy et al., Trends in Biotechnology 25(3):125-131, 2007

Plasmon-induced crystal growth @hotspots

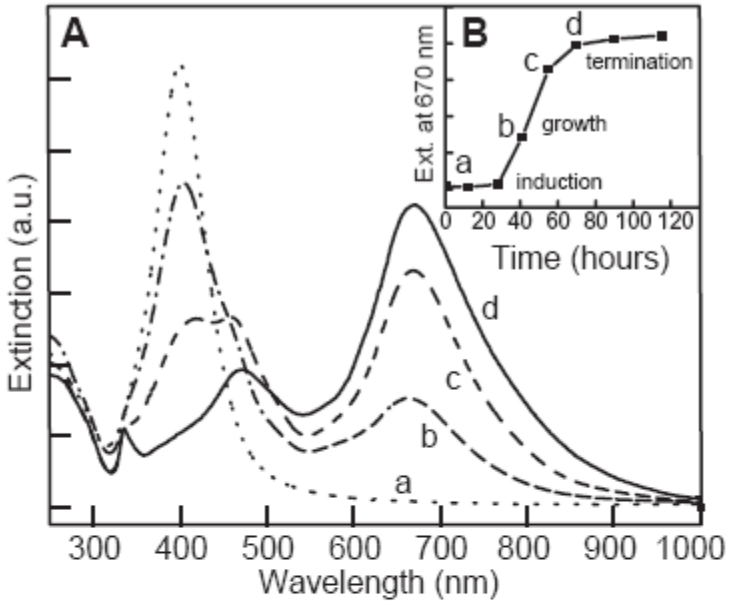

Fig. 1. (**A**) Time-dependent UV-Vis spectra showing the conversion of silver nanospheres to nanoprisms (a) before irradiation and after (b) 40, (c) 55, and (d) 70 hours of irradiation. (**B**) Corresponding extinction profiles at 670 nm as a function of time.

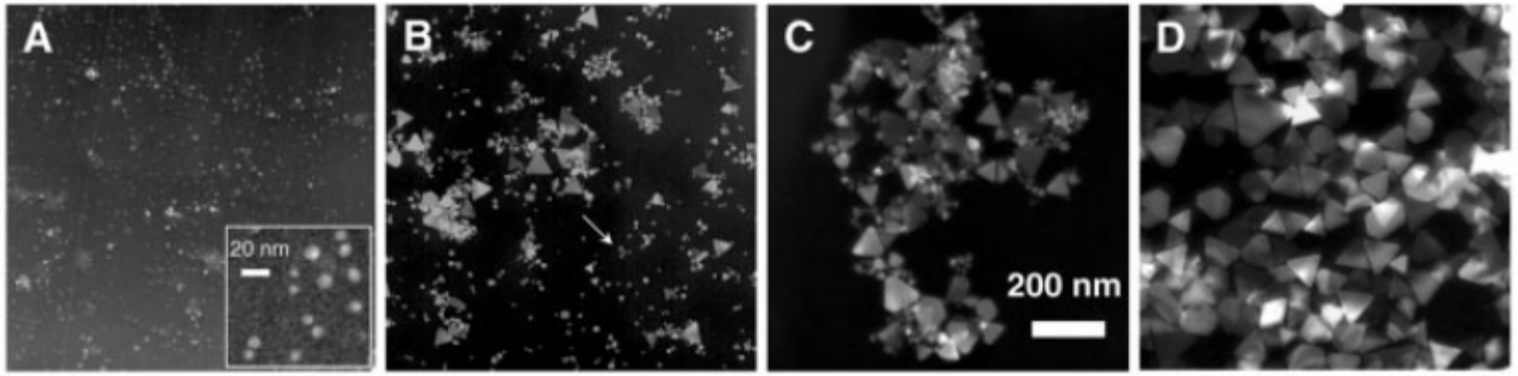

Fig. 2. TEM images (reverse print) mapping the morphology changes (**A**) before irradiation and after (**B**) 40, (**C**) 55, and (**D**) 70 hours of irradiation. Except for the inset in (A), the scale bar is 200 nm for all four images.

Jin et al., Science 294:1901-1903, 2001.

Emergence of a bimodal size distribution

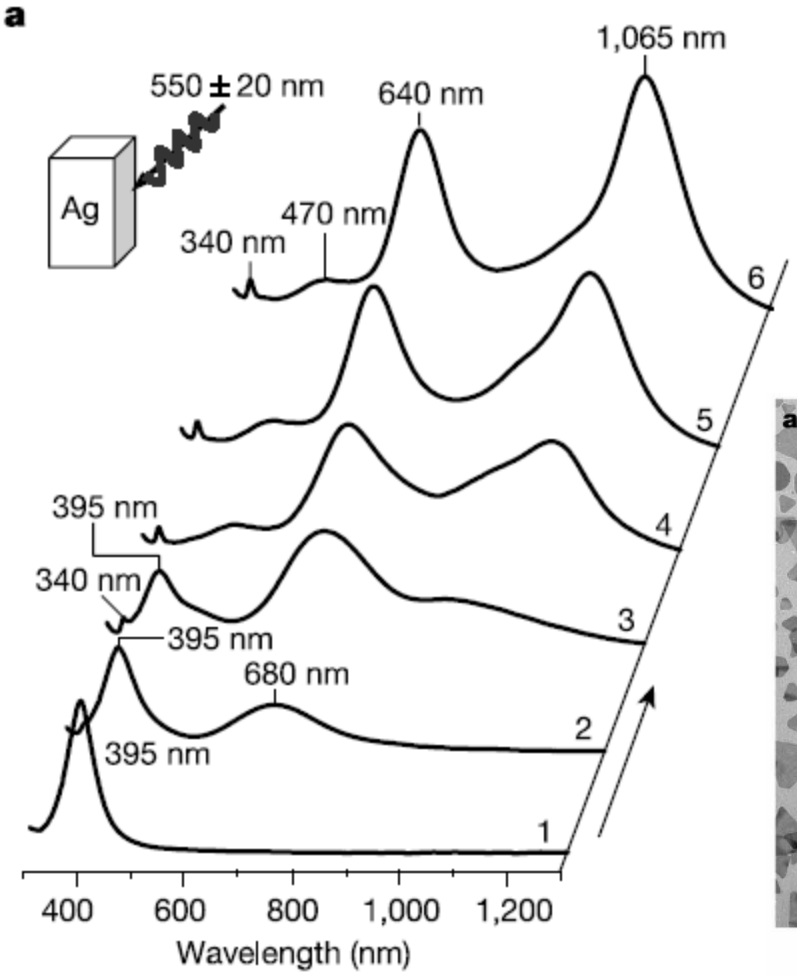

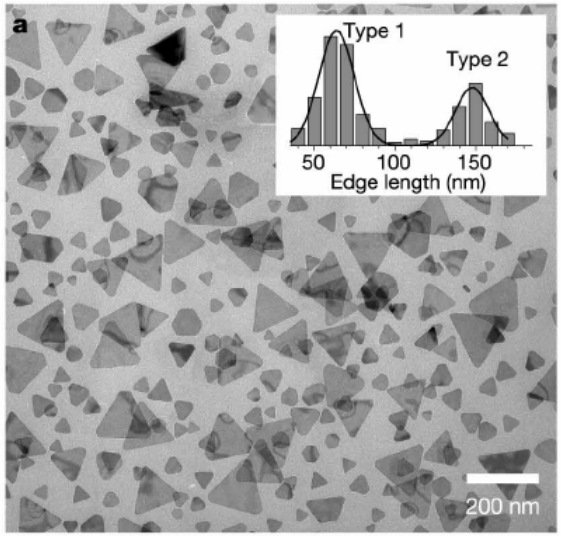

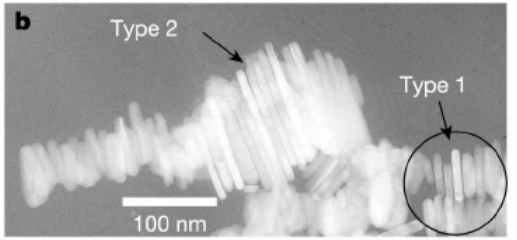

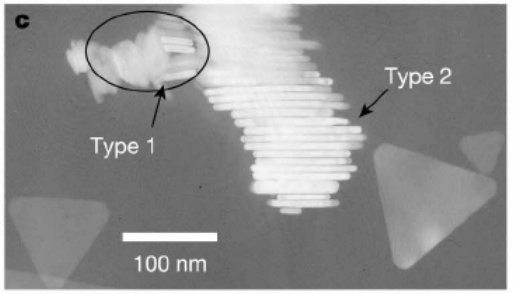

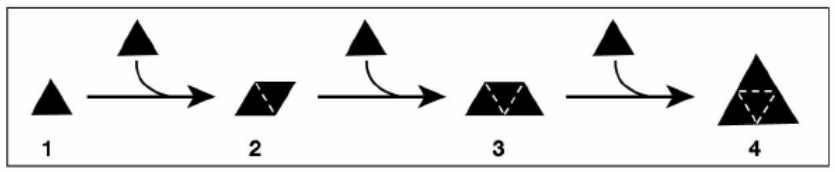

Jin et al., Nature 425:487-490, 2003.

Plasmonic "lithography"

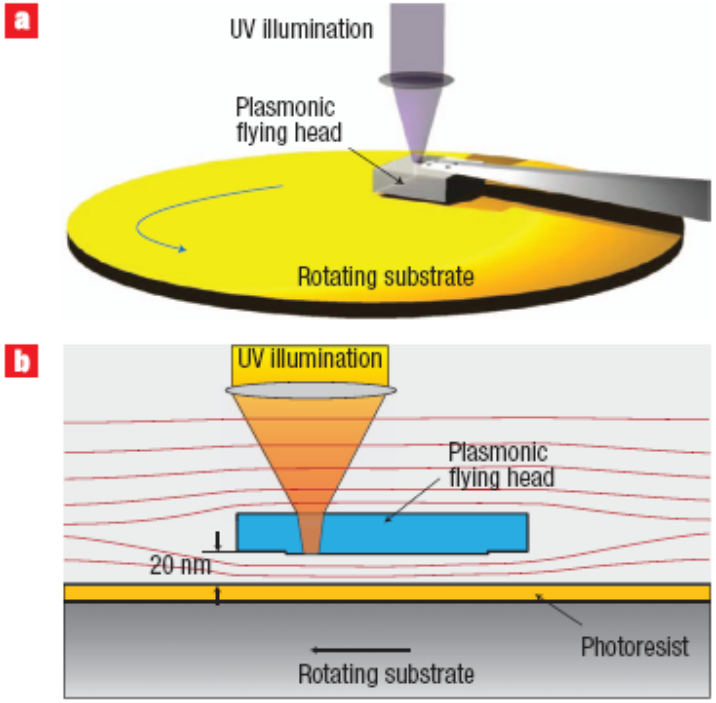

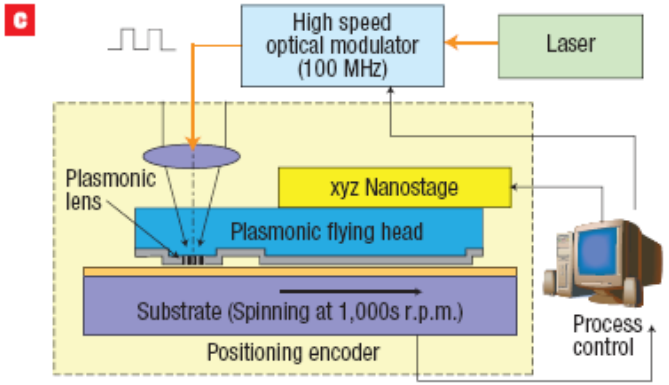

Figure 1 High-throughput maskless nanolithography using plasmonic lens arrays. a, Schematic showing the lens array focusing ultraviolet (365 nm) laser pulses onto the rotating substrate to concentrate surface plasmons into sub-100 nm spots. However, sub-100 nm spots are only produced in the near field of the lens, so a process control system is needed to maintain the gap between the lens and the substrate at 20 nm. **b**, Cross-section schematic of the plasmonic head flying 20 nm above the rotating substrate which is covered with photoresist. **c**, Schematic of process control system. The laser pulses are controlled by a high-speed optical modulator according to the signals from a pattern generator. The writing position is referred to the angular position of the disk from the spindle encoder and the position of a nano-stage along the radial direction.

Srituravanich et al., Nature Nanotechnology 3:733-737, 2008.

Plasmonic lenses

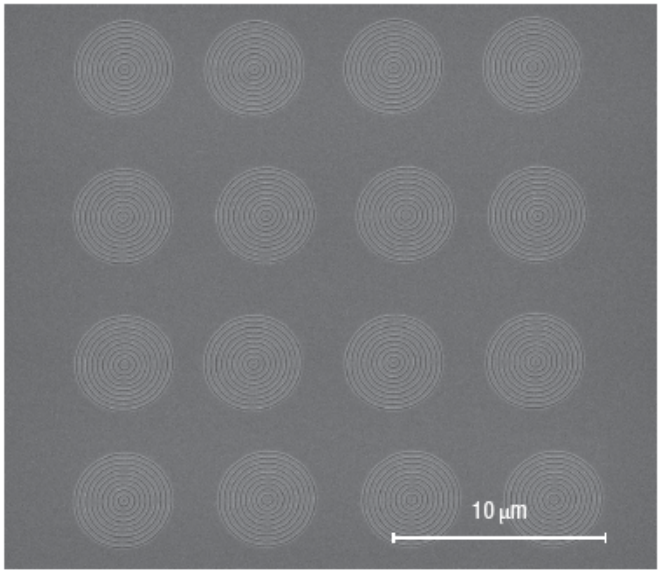

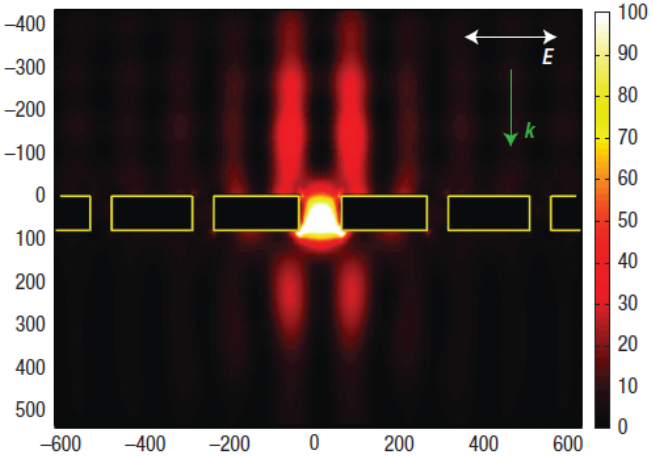

Patterns in TeOx photoresist)

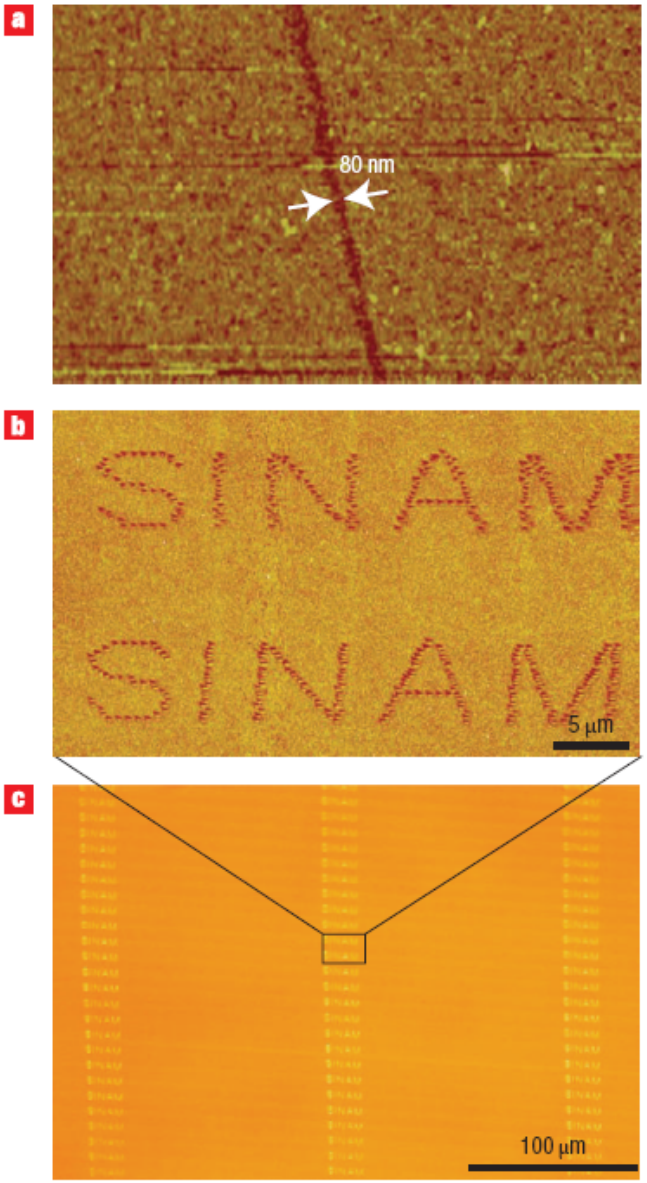

Srituravanich et al., Nature Nanotechnology 3:733-737, 2008.

Ultrafast laser heating via SPR

Timescales of interactions:

- Photon-electron ~pulse width
- Electron-electron ~100-500 fs
- Electron-phonon ~1-10 ps
- Ballistic phonon ~10-100 ps
- Diffusion ~100 ps

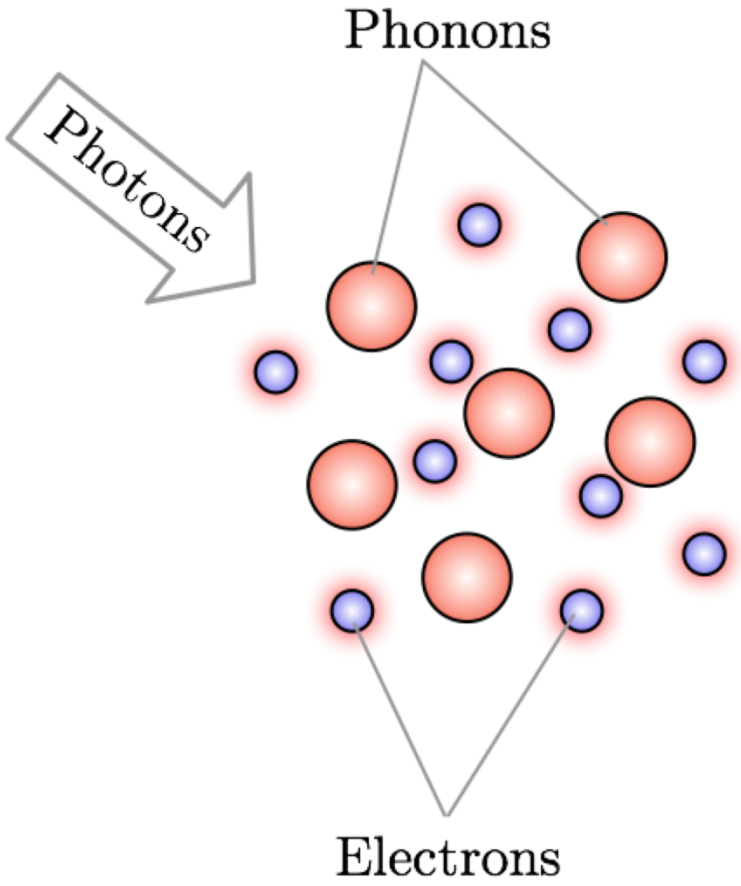

Application: Gold nanorods for tumor hyperthermia with pulsed lasers

Controlled size

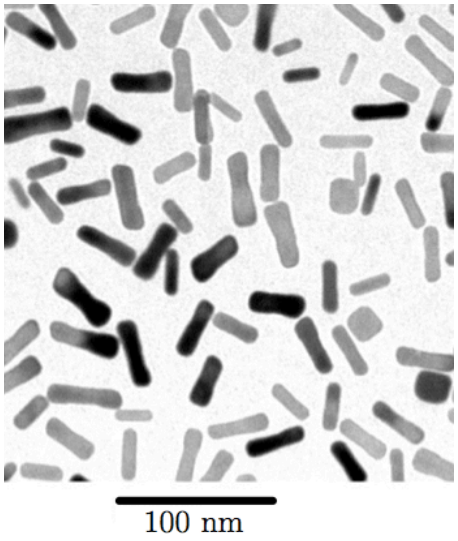

Tunable absorption spectra

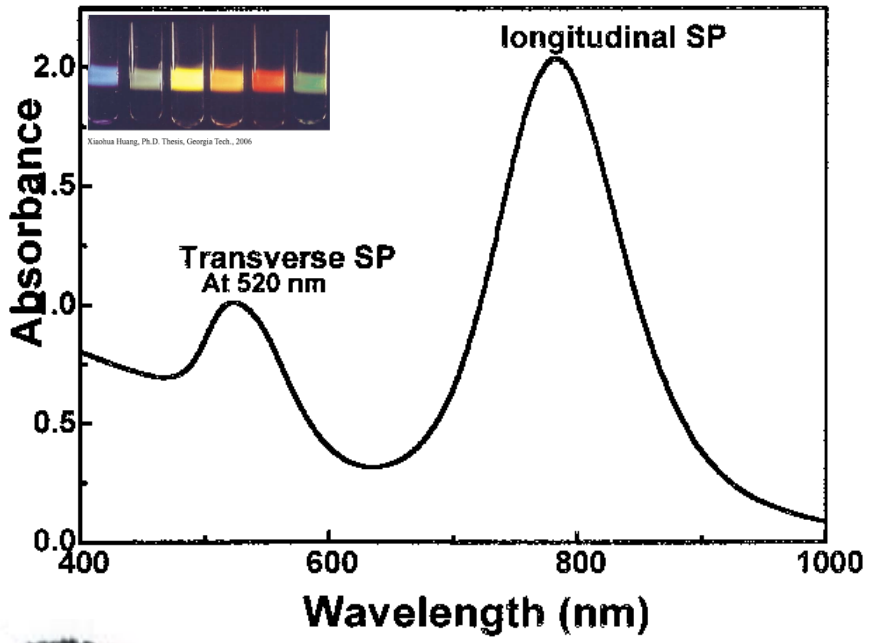

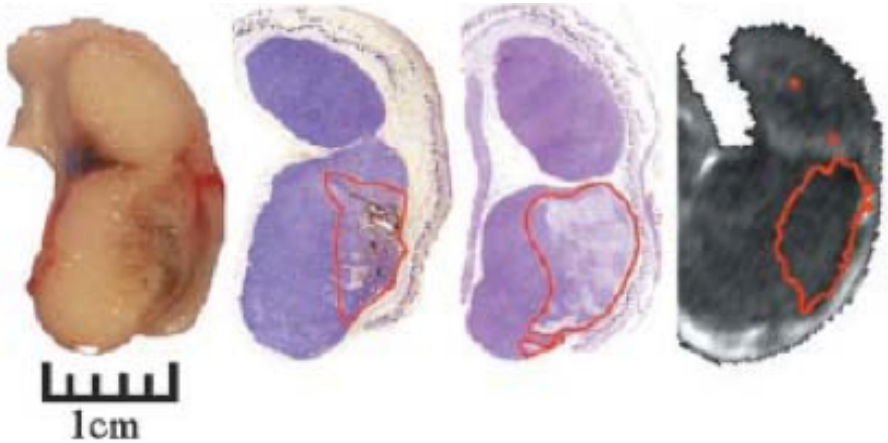

Xiaohua Huang, Ph.D. Thesis, Georgia Tech., 2006

Selectively bound to tumors, and then heat

Coating the nanorods

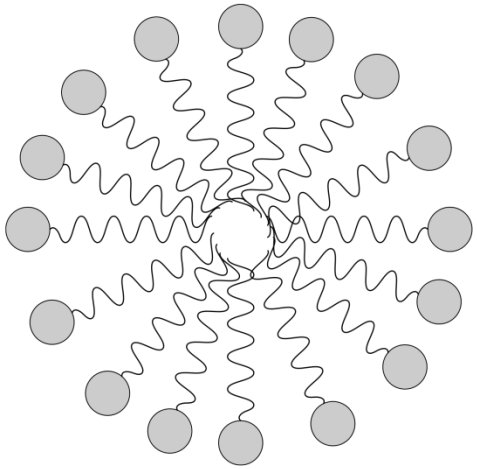

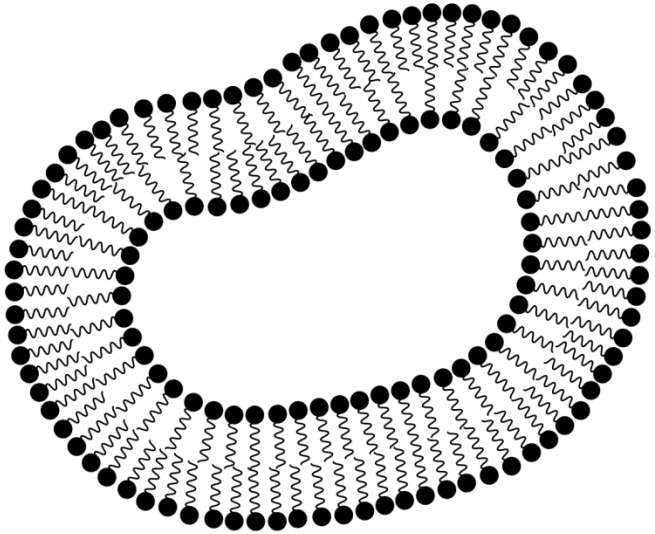

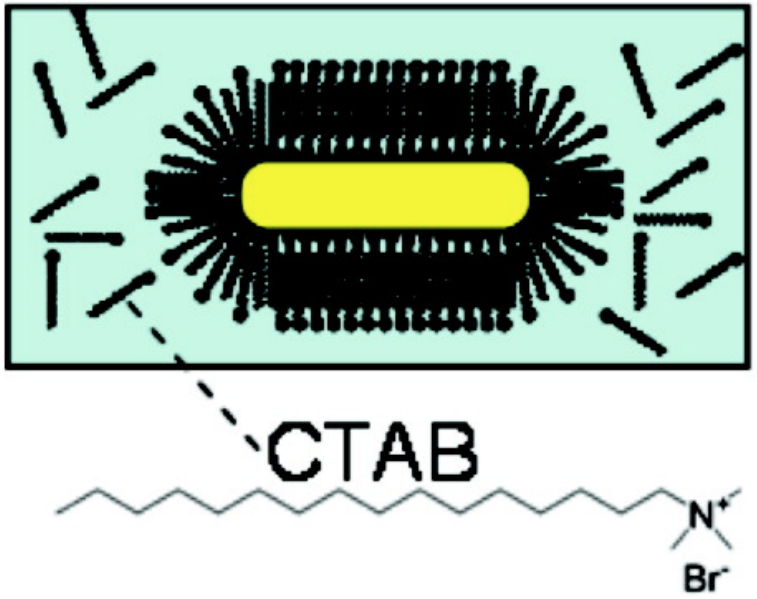

Ultrafast absorption and cooling from laser pulse

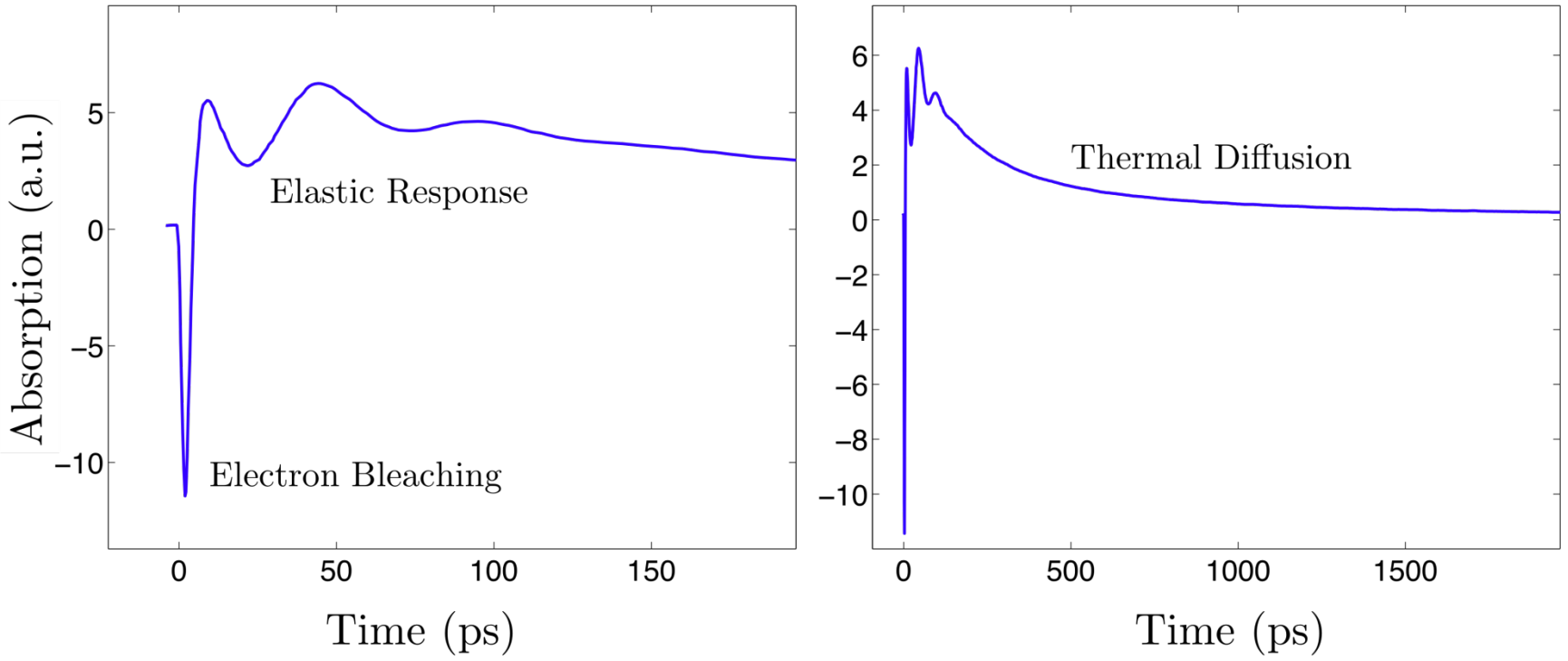

Measuring the effect of the bilayer with SPR

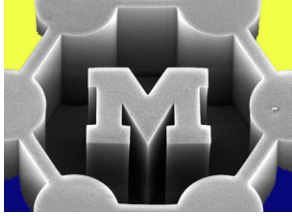

Bilayer forms with increased concentration

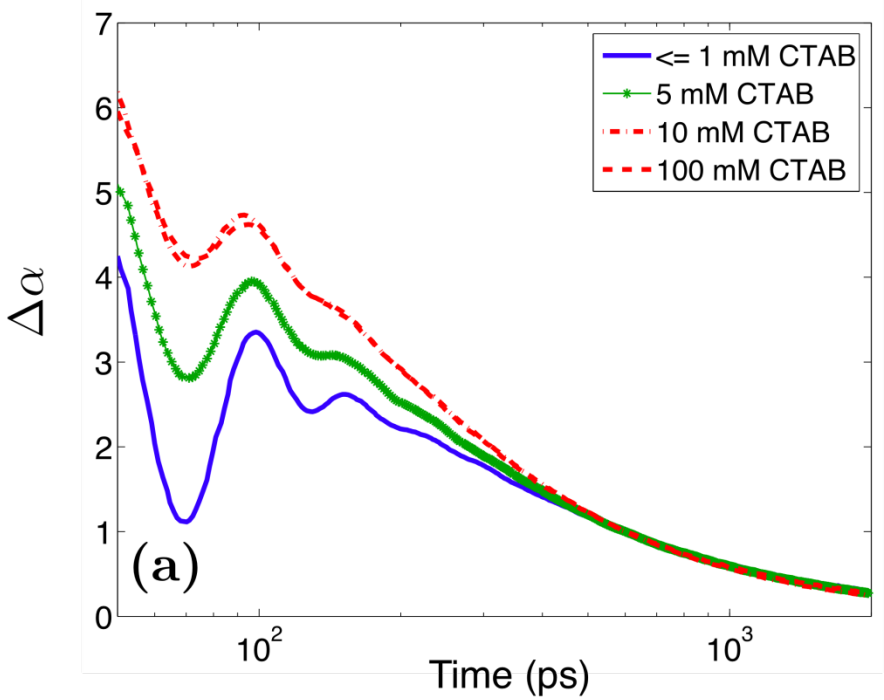

Bilayer decreases G, red-shifts the longitudinal SPR

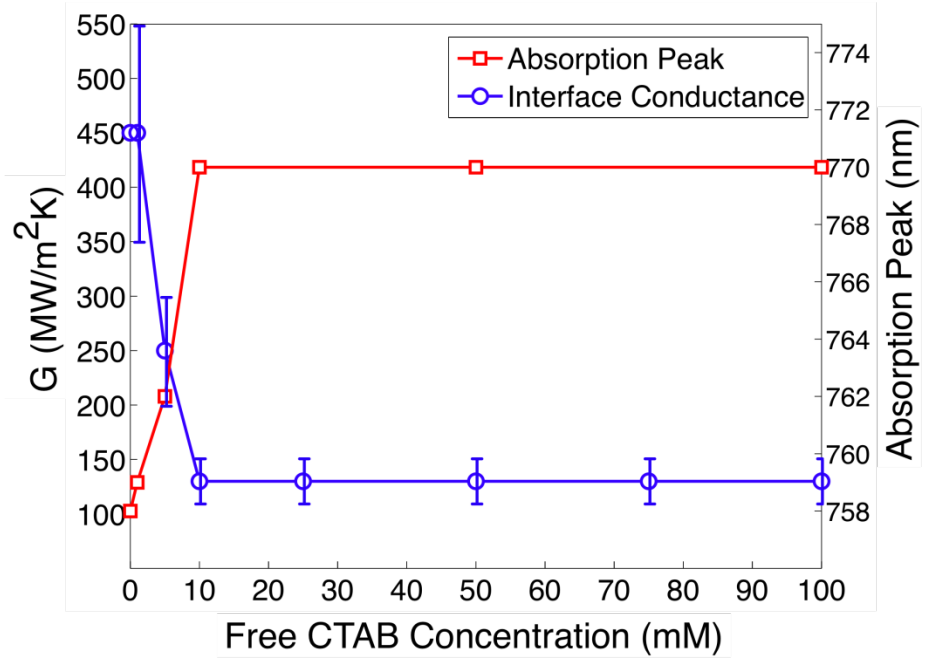

Schmidt et al., Journal of Physical Chemistry C, 112(35), 13320-13323, 2008